

## This is to certify that the

thesis entitled

Reactions of Dinuclear Transition Metal Antitumor Complexes with the DNA Model Nucleobase 9-Ethylguanine

Kemal V. Catalan

has been accepted towards fulfillment of the requirements for

MS degree in Chemistry

in Mexico

Date 2/26/99

# LIBRARY Michigan State University

PLACE IN RETURN BOX to remove this checkout from your record.

TO AVOID FINES return on or before date due.

MAY BE RECALLED with earlier due date if requested.

DATE DUE	DATE DUE	DATE DUE

6/01 c:/CIRC/DateDue.p65-p.15

## REACTIONS OF DINUCLEAR TRANSITION METAL ANTITUMOR COMPLEXES WITH THE DNA MODEL NUCLEOBASE 9-ETHYLGUANINE

By

## Kemal Vatansever Catalan

### **A THESIS**

Submitted to

Michigan State University
in partial fulfillment of the requirements
for the degree of

**MASTER OF SCIENCE** 

**Department of Chemistry** 

1999



#### Abstract

## REACTIONS OF DINUCLEAR TRANSITION METAL ANTITUMOR COMPLEXES WITH THE DNA MODEL NUCLEOBASE 9-ETHYLGUANINE

### By

#### Kemal V. Catalan

Mononuclear transition metal compounds such as cisplatin, iproplatin and carboplatin are well known for their extraordinarily high carcinostatic activity. Years of research have been devoted to the elucidation of their mechanism of action. The generally accepted model is the inhibition of DNA replication by the covalent binding of two adjacent guanine bases through their respective N<sup>7</sup> atoms to the platinum metal center. Other transition metal compounds are known to exhibit considerable anticancer activity that is also attributed to direct metal-DNA interactions. In this vein, we are investigating the preferred DNA binding sites as well as the exact binding modes of dinuclear transition metal carboxylates of the type M<sub>2</sub>(O<sub>2</sub>CR)<sub>4</sub>, M<sub>2</sub>X<sub>4</sub>(O<sub>2</sub>CR)<sub>2</sub> and M<sub>2</sub>(DTolF)<sub>2</sub>(O<sub>2</sub>CCF<sub>3</sub>)<sub>2</sub> (M = Ru, Rh and Re; R = CH<sub>3</sub>, CH<sub>2</sub>,CH<sub>3</sub>, CH<sub>2</sub>CH<sub>2</sub>CH<sub>3</sub>; DTolF = di-p-tolylformamidinate; X = halide). Recent studies in our laboratories have elucidated unprecedented bridging modes for the model nucleobases 9-ethylguanine and 9-ethyladenine. In addition, the synthesis and spectroscopic characterization of the reaction products of these metal compounds with the twelve base pair oligonucleotide, d(5'-CCT CTG GTC TCC-3'), have been performed. Other studies involving the polymerase chain reaction (PCR) indicate that the DNA replication process is inhibited by covalent metal binding to the template strand. The PCR results along with <sup>1</sup>H NMR spectroscopic, HPLC and X-ray crystallographic results will be presented.

## **TABLE OF CONTENTS**

	page
LIST OF ABBREVIATIONS	
CHAPTER I. INTRODUCTION	1
	2
	3
B. Intrastrand Cross-links	
8	
C. Interstrand Cross-links	•••••
10	
2. Proposed Design Strategies	12
3. Dinuclear Metal Complexes	13
A. Dinuclear Rhodium Complexes	14
B. Dinuclear Rhenium Complexes	16
CHAPTER II. DIRHODIUM ANTICANCER AGENTS	19
1. Introduction	20
2. Experimental	25
A. Synthesis	25
(1) Preparation of Rh <sub>2</sub> ( $\mu$ -DTolF) <sub>2</sub> ( $\mu$ -9-EtGH) <sub>2</sub> (O <sub>2</sub> CCF <sub>3</sub> ) <sub>2</sub> (1)	25
(2) Preparation of Rh <sub>2</sub> (μ-DPhF) <sub>2</sub> (μ-9-EtGH) <sub>2</sub> (O <sub>2</sub> CCF <sub>3</sub> ) <sub>2</sub> (2)	26
(3) Preparation of [Rh <sub>2</sub> (μ-DTolF) <sub>2</sub> (CH <sub>3</sub> CN) <sub>6</sub> ][BF <sub>4</sub> ] <sub>2</sub> (3)	26
(4) Preparation of [Rh <sub>2</sub> (μ-DTolF) <sub>2</sub> (μ-9-EtGH) <sub>2</sub> (CH <sub>3</sub> CN) <sub>6</sub> ][BF <sub>4</sub>	4]2 <b>(4)</b>
	27
(5) Synthesis of [Rh <sub>2</sub> (μ-DTolF) <sub>2</sub> (μ-9-EtGH) <sub>2</sub> (CH <sub>3</sub> CN) <sub>6</sub> ][BPh <sub>4</sub>	] <sub>2</sub> (5)
, , , , , , , , , , , , , , , , , , ,	27

B. X-ray Crystallography	27
(1) [Rh <sub>2</sub> (µ-DTolF) <sub>2</sub> (CH <sub>3</sub> CN) <sub>6</sub> ][BF <sub>4</sub> ] <sub>2</sub> (3)	28
(2) $[Rh_2(\mu-DTolF)_2(\mu-9-EtGH)_2(CH_3CN)_6][BF_4]_2$ (4)	29
C. 103Rh NMR Spectroscopy	29
3. Results 3	30
A. Spectroscopic Properties of (1) and (2)	30
B. Spectroscopic and Crystallographic Properties of (3)	35
C. Spectroscopic and Crystallographic Properties of (4)	42
D. <sup>103</sup> Rh NMR Spectroscopy	43
(1) Theory 4	13
(2) Results 4	19
4. Conclusion 5	50
CHAPTER III. DIRHENIUM ANTICANCER AGENTS	55
1. Introduction5	6
2. Experimental 5	57
A. Synthesis5	57
(1) Preparation of <i>cis</i> -Re <sub>2</sub> (μ-9-EtG) <sub>2</sub> Br <sub>4</sub> (6)	58
(2) Preparation of Re <sub>2</sub> ( $\mu$ -9-EtG) <sub>2</sub> ( $\mu$ -O <sub>2</sub> CCH <sub>3</sub> ) <sub>4</sub> Cl <sub>2</sub> (7)	58
(3) Preparation of Re <sub>2</sub> ( $\mu$ -9-EtG) <sub>2</sub> ( $\mu$ -O <sub>2</sub> CCH <sub>2</sub> CH <sub>3</sub> ) <sub>4</sub> Cl <sub>2</sub> (8a)	59
(4) Preparation of Re <sub>2</sub> ( $\mu$ -9-EtG) <sub>2</sub> ( $\mu$ -O <sub>2</sub> CCH <sub>2</sub> CH <sub>3</sub> ) <sub>4</sub> (BF <sub>4</sub> ) <sub>2</sub> ( <b>8b</b> )	59
(5) Preparation of Re <sub>2</sub> ( $\mu$ -9-EtG) <sub>2</sub> ( $\mu$ -O <sub>2</sub> CCH <sub>2</sub> CH <sub>3</sub> ) <sub>4</sub> (SO <sub>4</sub> ) (8c)	59
(6) Preparation of Re <sub>2</sub> ( $\mu$ -9-EtG) <sub>2</sub> ( $\mu$ -O <sub>2</sub> CC <sub>6</sub> H <sub>5</sub> ) <sub>2</sub> (CH <sub>3</sub> CN) <sub>2</sub> (BF <sub>4</sub>	(9) <sub>2</sub> (9)
	60
B. X-ray Crystallography6	60
(1) cis-Re <sub>2</sub> (μ-O <sub>2</sub> CCH <sub>2</sub> CH <sub>3</sub> ) <sub>2</sub> Br <sub>4</sub> (DMF) <sub>2</sub> ( <b>10</b> )	60
3. Results6	51
A. Crystallographic Determination of (10)	61

B. Spectroscopic Properties of (6)	62
C. Spectroscopic Properties of (7)	70
D. Spectroscopic Properties of (8)	71
E. Spectroscopic Properties of (9)	73
4. Conclusion	74
LIST OF REFERENCES	80

## **Abbreviations**

Å Angström

br broad

β Bohr magneton

cm-1 wavenumber

oC degree centigrade

d doublet (NMR), day, deuterated

 $\delta$  parts per million (ppm)

ε molar extinction coefficient

 $\lambda$  wavelength

g gram

mol mole

mmol millimole

h hour

IR infrared

J coupling constant (NMR)

k Boltzmann constant

MHz megaHertz

M mole per liter

m medium, multiplet

mL milliliter

μ bridging ligand

nm nanometer

NMR nuclear magnetic resonance

v frequency

ppm parts per million

s singlet, strong

TMS tetramethylsilane

UV ultraviolet

w weak X halide

DNA deoxyribonucleic acid

RNA ribonucleic acid

G guanosine

A adenosine

ade adenine or substituted adenine bases

d(pGpG) dimer of DNA containing guanine

9-EtGH 9-ethylguanine

9-EtAH 9-ethyladenine

9-EtG- 9-ethylguanine deprotonated at the N1 position

9-EtA<sup>-</sup> 9-ethlyadenine deprotonated at the N6 position

DTolF- N,N'-p-tolyformamidinate

DPhF- N,N'-diphenylformamidinate

form both DTolF- and DPhF-

S donor solvent

L ligands

## LIST OF TABLES

e				
foi				
for				
(9-				
3r				
foi				
LIST OF EQUATIONS				
in				
if				
•				

## LIST OF FIGURES

Figure 1	Schematic representation of cisplatin2
Figure 2.	Schematic representation of DNA4
Figure 3.	Pathway of hydrolysis of cisplatin7
Figure 4.	Schematic representation of inter- and intrastrand
	cross-links9
Figure 5.	Pathway of C2'-endo to C3'-endo conformational change.10
Figure 6.	Shcematic representation of other antitumor active platinum
	compounds11
Figure 7.	Schematic representation of dinuclear carboxylates14
Figure 8.	Schematic representation of "head-to-head" and "head-to-tail"
	isomers21
Figure 9.	Schematic representation of Rh <sub>2</sub> (μ-DTolF) <sub>2</sub> (O <sub>2</sub> CCF <sub>3</sub> ) <sub>2</sub> S <sub>2</sub> 22
Figure 10.	Schematic representation of Rh <sub>2</sub> (μ-DTolF) <sub>2</sub> (O <sub>2</sub> CCF <sub>3</sub> ) <sub>2</sub> (ade)
	23
Figure 11.	Schematic representation of $Rh_2(\mu\text{-DTolF})_2(O_2CCF_3)_2A24$
Figure 12.	Schematic representation of the "head-to-head" and "head-to-
	tail" isomers of Rh <sub>2</sub> ( $\mu$ -DTolF) <sub>2</sub> ( $\mu$ -9-EtGH) <sub>2</sub> (O <sub>2</sub> CCF <sub>3</sub> ) <sub>2</sub> 32
Figure 13.	<sup>1</sup> H NMR spectrum of Rh <sub>2</sub> (μ-DTolF) <sub>2</sub> (μ-9-
	EtGH) <sub>2</sub> (O <sub>2</sub> CCF <sub>3</sub> ) <sub>2</sub> 32
Figure 14.	Shcematic representation of deprotonated 9-ethylguanine34
Figure 15.	ORTEP diagram of $[Rh_2(\mu-DTolF)_2(CH_3CN)_6]^{2+}$ 37
Figure 16.	PLUTO diagram depicting the torsion angles of [Rh <sub>2</sub> (μ-
	DTolF) <sub>2</sub> (CH <sub>3</sub> CN) <sub>6</sub> ] <sup>2+</sup> 39
Figure 17.	<sup>1</sup> H NMR spectrum of [Rh <sub>2</sub> (μ-DTolF) <sub>2</sub> (μ-9-
	EtGH) <sub>2</sub> (CH <sub>3</sub> CN) <sub>2</sub> ] <sup>2+</sup> 44

Figure 18.	'H NMR spectrum of $[Rh_2(\mu-DTolF)_2(\mu-9-\mu)]$
	EtGH) <sub>2</sub> (CH <sub>3</sub> CN) <sub>2</sub> ] <sup>2+</sup> depicting the separation of the two
	isomers45
Figure 19.	<sup>1</sup> H NMR spectrum of [Rh <sub>2</sub> (μ-DTolF) <sub>2</sub> (μ-9-
	EtGH) <sub>2</sub> (CH <sub>3</sub> CN) <sub>2</sub> ] <sup>2+</sup> depicting the separation of the two
	isomers
Figure 20.	<sup>103</sup> Rh NMR chemical shift ranges49
Figure 21.	<sup>103</sup> Rh NMR spectra of Rh <sub>2</sub> (μ-DTolF) <sub>2</sub> (O <sub>2</sub> CCF <sub>3</sub> ) <sub>2</sub> S <sub>2</sub> and Rh <sub>2</sub> (μ-
	DTolF) <sub>2</sub> (μ-9-EtGH) <sub>2</sub> (O <sub>2</sub> CCF <sub>3</sub> ) <sub>2</sub>
Figure 22.	$^{103}$ Rh NMR spectrum of [Rh <sub>2</sub> ( $\mu$ -DTolF) <sub>2</sub> (CH <sub>3</sub> CN) <sub>6</sub> ] <sup>2+</sup> 53
Figure 23.	Schematic representation of dirhenium carboxylates56
Figure 24.	PLUTO diagram of cis-Re <sub>2</sub> (μ-O <sub>2</sub> CCH <sub>2</sub> CH <sub>3</sub> ) <sub>2</sub> Br <sub>4</sub> (DMF) <sub>2</sub> 63
Figure 25.	Schematic representation of the possible isomers of cis-Re <sub>2</sub> (µ-
	9-EtG) <sub>2</sub> Br <sub>4</sub> 65
Figure 26.	<sup>1</sup> H NMR spectrum of <i>cis</i> -Re <sub>2</sub> (μ-9-EtG) <sub>2</sub> Br <sub>4</sub> 66
Figure 27.	Pathway depicting the cis to trans isomerization of the
	dirhenium bis-carboxylates67
Figure 28.	Schematic representation of the extended structure of of cis-
	Re <sub>2</sub> (μ-9-EtG) <sub>2</sub> Br <sub>4</sub> 69
Figure 29.	Possible pathway for the deprotonation of 9-EtGH75
Figure 30.	$^{1}H$ NMR spectrum of Re <sub>2</sub> ( $\mu$ -9-EtG) <sub>2</sub> ( $\mu$ -O <sub>2</sub> CCH <sub>3</sub> ) <sub>4</sub> Cl <sub>2</sub> 76
Figure 31.	<sup>1</sup> H NMR spectrum of Re <sub>2</sub> (μ-9-EtG) <sub>2</sub> (μ-O <sub>2</sub> CCH <sub>2</sub> CH <sub>3</sub> ) <sub>4</sub> (BF <sub>4</sub> ) <sub>2</sub>
	77
Figure 32.	
	$O_2CC_6H_5)_2(CH_3CN)_2(BF_4)_2$ 79

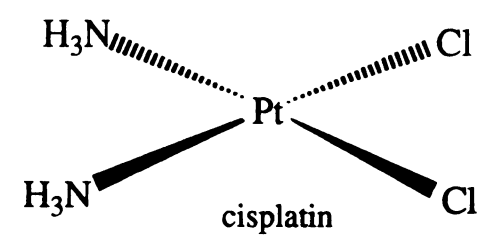
Chapter I

Introduction

### 1. Introduction

The development of cisplatin (Figure 1) for the chemotherapeutic treatment of testicular and ovarian cancers, as well as tumors of the bladder, head and neck has stimulated investigation of the antitumor activity of a wide range of mononuclear platinum complexes. 1 This explosion of research is due, in part, to the extremely high toxicity observed for cisplatin. Cancer patients who are administered cisplatin are threatened by a range of toxic side effects including nephrotoxicity, myeolosuppression, ototoxicity, nausea, peripheral neuropathies and cardiac abnormalities. Obviously, less dangerous treatments are sought so that such health risks can be minimized. An equally compelling reason for further research into cisplatin and related compounds is the possibility of identifying compounds that may target cancers not affected by cisplatin, e.g. deadly tumors such as lung and colon cancers. Furthermore, recent studies suggest that cisplatin itself exhibits carcinogenic effects, although the extent of carcinogenicity in humans is unknown.<sup>4</sup> The challenge now faced is to tailor and design inorganic complexes with improved biological activity and resistance to physiological decomposition, with concomitant reduction of toxic side effects.

Figure 1



## A. Mechanism of Action of Cisplatin

Before contemplating potential candidates as antitumor drugs it is important to first understand the accepted mechanism of action of cisplatin, and to give a general description of DNA. In the nucleus of a cell, DNA is coiled around histone proteins which help to organize DNA into a chromatin-like structure.<sup>1,8</sup> This chromatin-like structure consists of two strands coiled into a double helix. A single strand contains the nucleotide bases guanine, adenine, cytosine, and thymidine linked together by a sugarphosphate backbone (deoxyribose). The two strands run in opposite directions with respect to each other, and are linked by Watson-Crick hydrogen bonding of the base pairs: guanine with cytosine and adenine with thymine (Figure 2).<sup>1,8</sup> When transcription and replication occur, the two strands must unravel, thereby separating the hydrogen-bonding of the base pairs.

While the accepted mechanism of cisplatin is not fully understood, evidence supports the conclusion that DNA interactions are responsible for its activity. It is not known, however, whether platination of DNA is the sole cellular event that leads to the death of tumor cells. Experiments that measure the rates of DNA, RNA, and protein syntheses in cisplatin-treated cells reveal that DNA synthesis is preferentially inhibited, while RNA and protein syntheses are only slightly affected.<sup>5</sup> Although cisplatin has been observed to interact with proteins, cell wall components and the sugarphosphate backbone, the platination of B-DNA (the classical structure of the double helix) at the purines is thought to inhibit cell growth by creating irreparable lesions on the DNA strands of tumor cells.<sup>6,7</sup>

Figure 2

Table  $1^{7}$ 

Purine Purine	<u>Site</u>	pK <sub>a</sub> Range
Guanine	N7	2.3
Guanine	N1	9.3
Guanine	N3	?
Adenine	<b>N</b> 7	-1.5
Adenine	N1	3.7
Adenine	N6a	?
Cytosine	N3	4.4
Cytosine	<b>N</b> 4	?
Uracil	N3	9.5
Thymine	N3	9.5

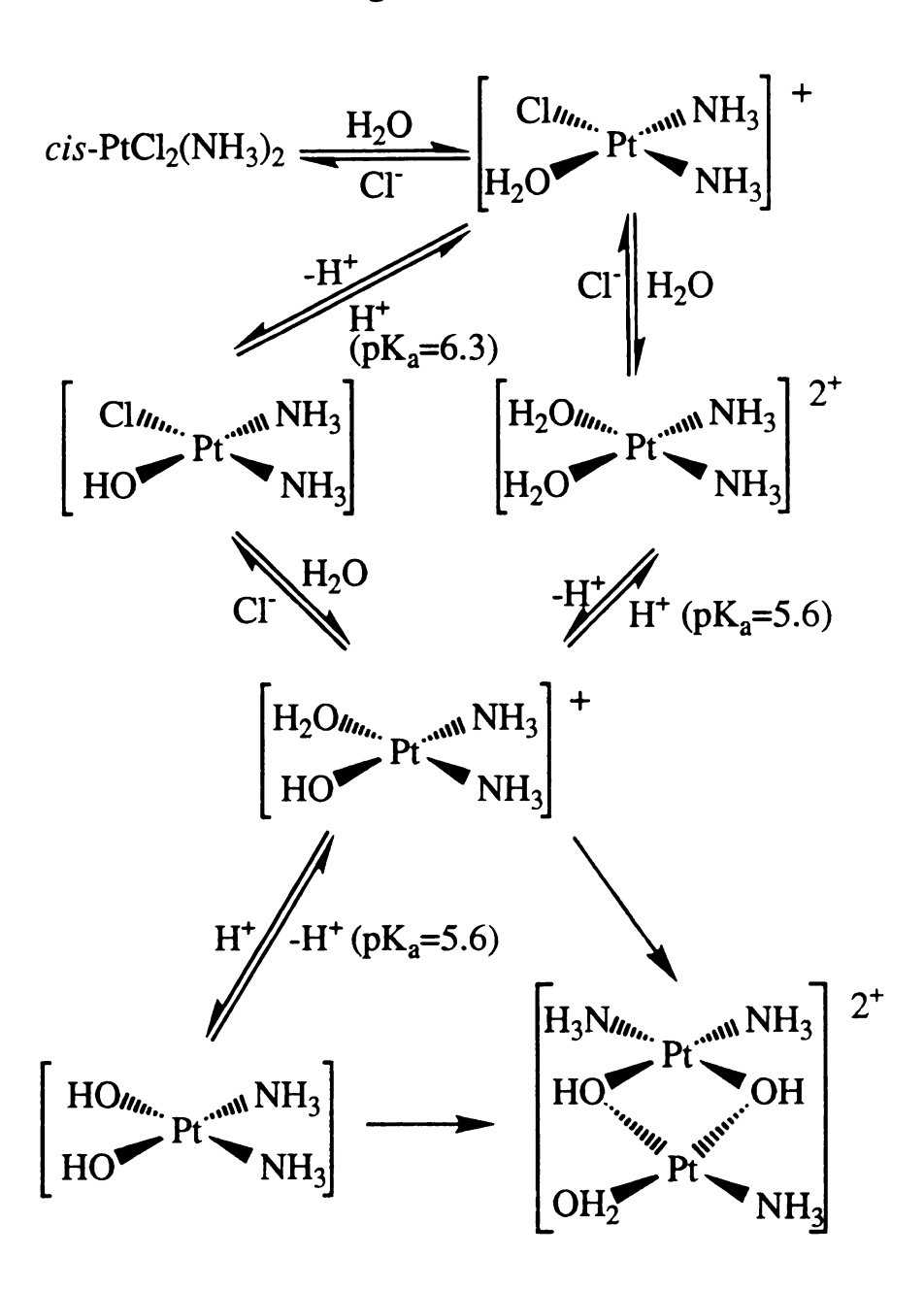
a = N6 is the exocyclic nitrogen after deprotonation

The observed coordination modes for Pt(II) to DNA bases are pH dependent (Table 1), with the N7 positions of guanine and adenine and N3 of cytosine and adenine being the preferred binding sites at neutral pH (which is approximately physiological pH). The N7 position of guanine has been determined by X-ray crystallographic and NMR studies to be the most likely site of coordination for platinum compounds. The guanine N1 and N3 positions become available for binding at a pK<sub>a</sub> of 9.3 with an excess of platinum compound. The two most common sites for binding at adenine

are the N7 and N1 positions. The pyrimidines are found to preferentially bind at the N3 position. Cytosine readily binds at N3, unlike thymine, which must first deprotonate before metallation can occur at this position. The main rationale for purine N7 positions being the frequently observed coordination sites in double helical DNA is the availability of this position which is exposed in the major groove, and their lack of involvement in Watson-Crick hydrogen bonding, especially in B-DNA. It has been noted in general, that guanine N7 is the preferred site of attack by platinum compounds for a variety of reactions. 1,2,6,7 The exocyclic amino- and keto- groups as well as the phosphate groups are possible sites for hydrogen-bonding to the ammonia ligands of bound cisplatin, a situation that would further disrupt the structure of the DNA coil, and aid in stabilization of the adducts. 7

One of the open questions in this field remains to be settled, namely what form of cisplatin actually binds to DNA? In any case, it is clear that the initial binding mode would be highly dependent on cell pH. Unfortunately, most of the present knowledge regarding the transport of cisplatin in living tissue is based on the behavior of the compound *in vitro*, which may be difficult to extrapolate to *in vivo* situations. For example, it is known that depending on the Cl- concentration and pH in the medium, cisplatin will undergo hydrolysis.<sup>6</sup> As depicted in Figure 3, cisplatin hydrolyzes in aqueous media and basic pH conditions to form aqua and hydroxo species. Due to the high Cl- concentration outside of the cell (~100 mM) hydrolysis is prevented. The Cl- concentration inside the cell, however, is considerably lower (~4 mM), a situation that facilitates the hydrolysis process.

Figure 3

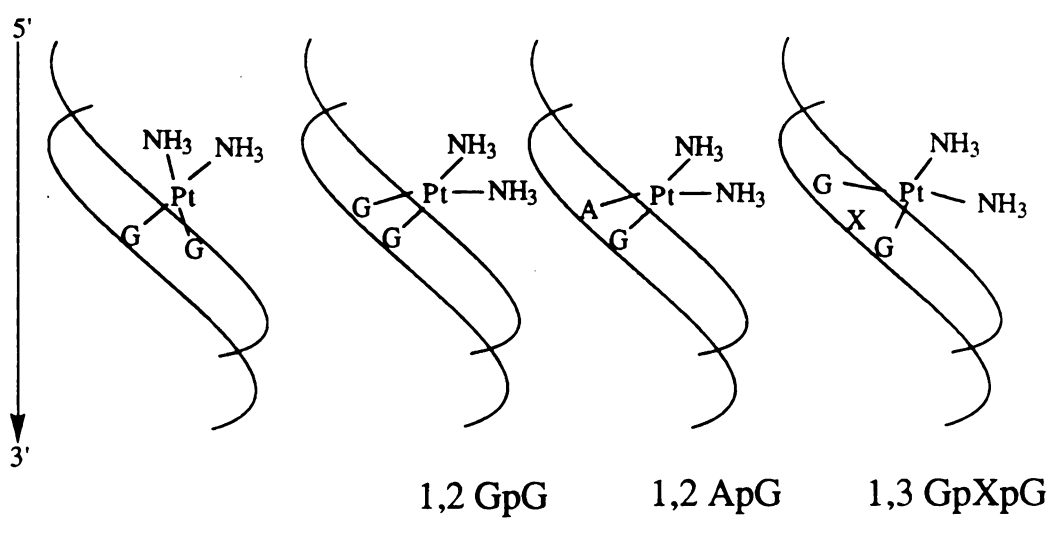


### B. Intrastrand Cross-links

It is known that the binding of hydrolyzed cisplatin to DNA promotes the unwinding and shortening of the double helix with the formation of two main binding modes; these are a short range intrastrand cross-link that is responsible for the unwinding effect and a long range cross-link that leads to the shortening of the strand.<sup>2,3,7</sup> Extensive, studies have confirmed that platination at the deoxyguanosine N7 atom bends the DNA in the direction of the major groove.<sup>3</sup>

After many years of research on the subject, researchers generally agree that the most common DNA platinum species is a bifunctional DNA adduct of general formula (NH<sub>3</sub>)<sub>2</sub>Pt(XpX) or (NH<sub>3</sub>)<sub>2</sub>Pt(XpNpX) where X is either guanosine (G) or adenosine (A), and N is any of the other DNA nucleosides.<sup>2</sup> Migration of bound cisplatin from one nucleobase to another has been found to be uncommon, and is thought to be an unlikely event under ambient conditions. A schematic of the four most common modes of binding exhibited by cisplatin is depicted in Figure 4. High resolution NMR, as well as X-ray crystallographic and chromatographic studies support the hypothesis that GpG is the preferred binding site as opposed to the other adducts. From the X-ray crystallographic studies performed on cis-[Pt(NH<sub>3</sub>)<sub>2</sub>(d(pGpG))], it was observed that a phosphate group can participate in hydrogen-bonding with one of the ammonia groups of cisplatin. Furthermore, the O6 position on the other purine is also in the range of hydrogen-bonding with a cisplatin ammonia ligand. The hydrogen-bonding disrupts the Watson-Crick base pairing leading to a subtle perturbation of the double helix.<sup>1</sup>

Figure 4



**Interstrand Crosslink** 

**Intrastrand Crosslink** 

G = guanine

A = adenine

X = cytosine (C), thymine (T), adenine (A)

It is important to note that the preferred direction of binding for the 1,2-intrastrand cross-linkage is also directed from the 5'-base to the 3'-neighbor. Similar binding modes were found for a 5'-deoxyguanosine directing the metal to a 3'-dX (X = C,T,A where deoxyadenosine was preferred). Studies predict that the shortening and unwinding of the double helical DNA occurs after the platinum chelation of a G-G sequence. This chelation causes a tilting of the G-G bases out of their parallel alignment. The tilting instigates a kink in the helix of about 40°-70°. Additional distortion occurs at the 5'-deoxyribose ring which changes from a C2'-endo to a C3'-endo ring puckering (Figure 5) to accommodate the strain caused by the cisplatin 1,2-intrastrand binding to a -GG-sequence.3,7,13,14

Figure 5

Long range 1,3-intrastrand cross-links have been attributed to a more prominent shortening of DNA.<sup>1,3,7</sup> Cisplatin adducts with d(GpCpG), d(GpApG) and d(GpGpG) all have been characterized for the 1,3-intrastrand type chelation. Both 1,3- and 1,2-intrastrand cross-links have been found for the adduct with d(GpGpG) where the 1,3-intrastrand binding is favored *in vivo*, although the 1,2-intrastrand cross-link is thought to be the more cytotoxic of the two. One of the explanations advanced for this is that the 1,3-intrastrand cross-links create a greater distortion in the double helix than the 1,2-type chelation, and large perturbations to DNA are more easily recognized by DNA repair enzymes than those that produce more subtle damage.<sup>2,15</sup>

## C. Interstrand Cross-linking

Interstrand cross-links have been found to account for less than 1% of the total amount of platinum bound to double-stranded DNA. The most prominent cross-link was found to be cisplatin bound to two deoxyguanosines at the guanine N7 position. It is important to note that the

major sequence in which the cross-link occurs is from the  $5' \rightarrow 3'$  end.<sup>12</sup> Although this mode of binding is not considered to be the primary DNA adduct of cisplatin responsible for tumor cell death, it certainly cannot be ruled out as an important binding mode for antitumor compounds.

In summary, studies have shown that *intra*-strand rather than *inter*-strand platinum chelation predominates. Clearly, cisplatin preferentially binds to guanine bases of DNA to form bifunctional d(GG) and d(GXG) adducts which are thought to be easily recognized by repair enzymes. Platination of deoxyguanosine may be preferred due to the availability of the exocyclic O6 to form hydrogen-bonds to cisplatin. This line of reasoning also helps to explain the lower degree of activity observed in the *trans* analogue which bends the double helix in two directions by preferentially forming 1,3-d(GXG) adducts. 16

Figure 6

$$CH_3$$
 $CH_3$ 
 $CH_3$ 
 $CH_3$ 
 $CH_4$ 
 $CH_5$ 
 $CH_5$ 
 $CH_5$ 
 $CH_5$ 
 $CH_5$ 
 $CH_7$ 
 $CH_7$ 

Spiroplatin

## 2. Proposed Design Strategies

Since the presence of DNA-bound platinum that disrupts the double helix conformation is considered cytotoxic to tumor cells, it is reasonable to expect that other metal compounds could produce the same disruption of the normal processes of transcription and DNA replication. Indeed antitumor activity has been recognized for a variety of platinum compounds including carboplatin, iproplatin, and spiroplatin (Figure 6) which have been extensively studied in clinical settings. In fact carboplatin has been recently approved for clinical use. 1 Carboplatin and spiroplatin are structurally similar to cisplatin in that they are square planar complexes with two cis-nitrogen donors. Iproplatin, on the other hand, is an octahedral Pt(IV) complex which is thought to undergo in vivo reduction to a square planar hydrolyzed Pt(II) complex. From the extensive mechanistic studies aimed at elucidating the effect of cisplatin DNA replication, and the collective studies of the mechanisms of similar platinum complexes, key trends have been discerned regarding the activity of inorganic antitumor compounds:

- (1) the complexes should be designed such that two *cis*, rather than *trans*, ligands substitute in reactions with biological molecules.
- (2) the complexes should be neutral compounds although they may become charged after ligand exchange in the body.
- (3) the geometry of the complexes should be square planar or octahedral.
- (4) the leaving groups should be ~3.4 Å apart on the molecule (the Watson-Crick ladder spacing).



- (5) the rates of exchange should fall into a narrow range of not occurring too rapidly, as this will result in decomposition of the compound before reaching the tumor cells, and not too slowly, as this will result in little or no activity.
- (6) the remaining groups across from the leaving groups should be robust, and preferably be capable of participating in hydrogen-bonding such as amines.<sup>17</sup>

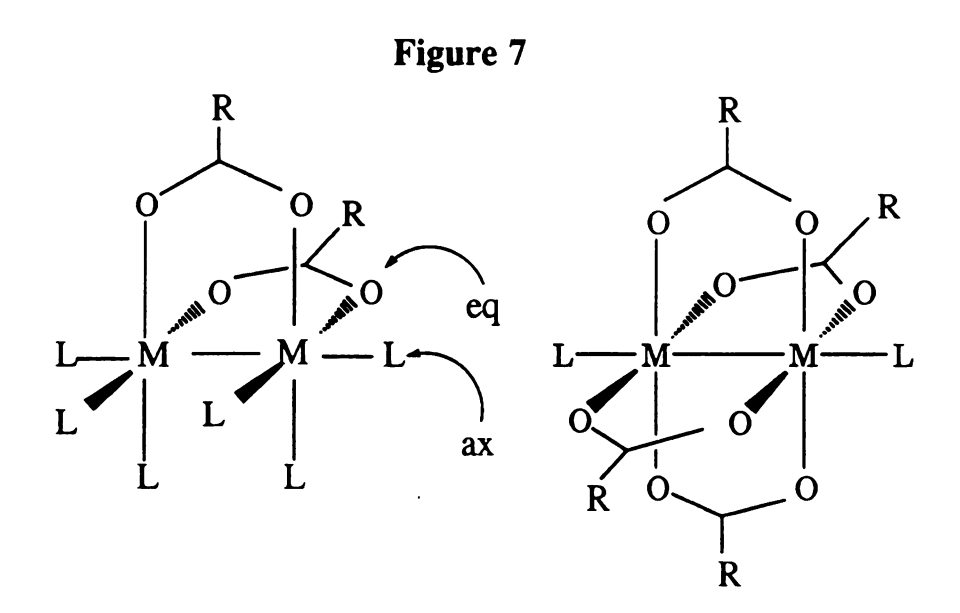
## 3. Dinuclear Metal Complexes

The search for transition metal complexes adhering to the criteria set forth by the collective efforts of researchers in the field has included a broad range of compounds. Following the discovery of the cytotoxic behavior of cisplatin, complexes of the other platinum group metals were among the first class of compounds tested for antitumor activity. In addition, cyclopentadienide complexes of Mo, Ti and V were also subjected to antitumor investigations. Other late transition metal compounds that have been studied include cis-[Ru(NH<sub>3</sub>)<sub>4</sub>Cl<sub>2</sub>]<sup>+</sup> and the trans isomer of RuCl<sub>2</sub>(DMSO)<sub>4</sub>.<sup>4</sup> In all of these studies, new compounds have been tested against the same tumor cell lines affected by cisplatin, which is unfortunate since this will lead only to new drugs for which treatments already exist.<sup>1</sup> For a completely different class of possible antitumor complexes, cancer cell lines other than those treatable by cisplatin must also be studied.

One entirely different class of antitumor active compounds whose structures and reactivities do not closely adhere to the cisplatin guidelines for anticancer compounds are dinuclear transition metal complexes of rhodium, ruthenium and rhenium. Compounds of these metals with



bridging carboxylate ligands have been studied as to their antitumor activity against various tumor cell lines with very promising results ensuing. To date, however, no major advances in the development of these compounds for pharmaceutical use have been made, most likely due to their specialized nature and their facile decomposition under physiological conditions. The so-called "lantern" structures of these compounds (depicted in Figure 7) allow for two possible types of binding sites, namely equatorial (eq) and axial (ax).



M = Re, Rh, Ru  $R = CF_3$ , alkyl  $L = Cl, Br, CH_3CN, CH_3OH$ 

## A. Dinuclear Rhodium Complexes

Dirhodium carboxylate compounds of the type  $Rh_2(O_2CR)_4L_2$  (R = CH<sub>3</sub>, CH<sub>2</sub>CH<sub>3</sub>, CH<sub>2</sub>CH<sub>3</sub>, CH<sub>2</sub>OCH<sub>3</sub>; L = donor solvent) exhibit considerable antitumor activity in mice bearing the Ehrlich ascites tumor.

These complexes were found to inhibit DNA but not RNA synthesis with dirhodium(II) tetrabutyrate being the most potent inhibitor. Studies indicate that these complexes bind to denatured DNA, poly-A, poly-G, ribonuclease AA, and bovine serum albumin. The same studies also concluded that the dirhodium tetracarboxylates do not bind to highly polymerized native calf thymus DNA, poly-G and poly-C. It was postulated from these preliminary observations that the observed antitumor activity was due to reversible binding by a nitrogen donor in the biomolecules through the axial position of the dimetal unit. Additional in vitro binding to purified DNA polymerase I and RNA polymerase I was also observed, but in vivo studies revealed only the interruption of DNA replication. It is questionable as to whether this inhibition was due to interactions with polymerase or to interactions with the DNA bases. 18a, b

Further studies of dirhodium tetracarboxylates binding to enzymes containing sulfhydryl (-SH) groups at or near the active site revealed that the binding occurs irreversibly to these molecule types. The rate of *in vivo* enzyme inactivation was in the order butyrate > propionate > acetate > methoxyacetate, which is correlated to the lipophilicity and solubility of the complexes which increases in the same order. The R group identity of the carboxylate ligands also has a direct affect on the Lewis acidity of the metal dimer. 18,20

A major question regarding the antitumor activity of dirhodium tetracarboxylates that occurred to us early on is whether the reactions indeed occur with only axial binding or equatorial binding to DNA nucleobases. It was postulated by other researchers that irreversible enzyme binding occurs by equatorial substitution of the carboxylate ligands which may be extrapolated to DNA studies, since this binding was found to

be irreversible in vivo. 18c,d This theory was brought into serious question in our laboratories several years ago when the feasibility of equatorial binding of DNA purines to the dirhodium unit was verified by X-ray crystallography for guanine (chapter 2), which adopts a previously unknown bridging mode across the Rh-Rh bond in the neutral compound Rh<sub>2</sub>(9-EtGH)<sub>2</sub>(O<sub>2</sub>CCH<sub>3</sub>)<sub>2</sub>(CH<sub>3</sub>OH)<sub>2</sub>. Two guanine bases span the dirhodium unit in a cis disposition and in a "head-to-tail" orientation of the N7-O6 atoms. <sup>1</sup>H NMR spectroscopic evidence supports a second isomer that is assumed to be the "head-to-head" arrangement which is the more biologically relevant adduct; attempts to characterize this adduct by X-ray crystallography are currently underway. 19 The neutral complex,  $Rh_2(O_2CCF_3)_4L_2$  (where L = CH<sub>3</sub>CN, CH<sub>3</sub>OH) yields products with 9-EtGH that exhibit the same bridging mode for the purines as the acetate derivative. In this case, the "head-to-head" and "head-to-tail" isomers of the purine are observed to be formed in a 1:1 ratio as judged by <sup>1</sup>H NMR spectroscopy in the H8 region. A similar situation is encountered with the partially solvated species [Rh<sub>2</sub>(O<sub>2</sub>CCH<sub>3</sub>)<sub>2</sub>(CH<sub>3</sub>CN)<sub>6</sub>]<sup>2+</sup> in reactions with 9-EtGH, from which the biologically relevant "head-to-head" isomer of the compound [Rh<sub>2</sub>(O<sub>2</sub>CCH<sub>3</sub>)<sub>2</sub>(9-EtGH)<sub>2</sub>]<sup>2+</sup> was isolated and characterized by X-ray crystallography. Similar bridging modes were also verified by crystallography for diruthenium tetracarboxylate compounds in reactions with 9-ethylguanine.<sup>19</sup>

## B. Dinuclear Rhenium Complexes

The literature regarding the biological activity of rhenium is sparse, with no known case of rhenium poisoning having been reported. As far as biologists are aware, rhenium is not a trace constituent in plants or animals. We noted with interest that several dinuclear complexes of rhenium have

been subjected to antitumor testing; these are the compounds Re2(O2CR)4SO4 (R=CH3, CH2CH3, CH2CH3) which were tested against sarcoma, melanoma, and leukemia cell lines in mice. tetrapropionate complex was observed to be far more effective than the tetraacetate and the more toxic tetrabutyrate against all three cell lines. It was found that high consecutive doses of [Re<sub>2</sub>(O<sub>2</sub>CCH<sub>2</sub>CH<sub>3</sub>)<sub>4</sub>]<sup>2+</sup> were necessary for inhibition of the melanoma and sarcoma tumors in mice. Leukopenia (decrease of white blood cell production) was observed in the leukemia bearing mice, but the same high doses needed for the inhibition of the tumors significantly pronounced the myelosuppressive effects.<sup>17</sup> Since it is known that the Re-Re quadruple bond of the cationic tetracarboxylate compounds is susceptible to decomposition to rhenium oxides in the presence of water, 17,26 it has been postulated that this could account for the necessity of high doses in order to observe antitumor activity. In other words, the compound is effective only if the rate of cytotoxicity is greater than the rate of hydrolysis.

More recently, a class of more stable carboxylate compounds of rhenium, the *cis* biscarboxylates, was observed to exhibit greater antitumor activity and even lower toxicities than the cationic tetracarboxylates. Although the complex *cis*-Re<sub>2</sub>(O<sub>2</sub>CCH<sub>2</sub>CH<sub>3</sub>)<sub>2</sub>X<sub>4</sub>(H<sub>2</sub>O)<sub>2</sub> (X = halogen) undergoes hydrolysis much slower than its tetracarboxylate analogue, the dose levels were still considered to be too high for further testing. Nevertheless, these results support the inhibition of DNA synthesis with no interactions occurring with proteins or RNA, which is a promising starting point for future generations of rhenium-based drugs.<sup>17b</sup>

Clearly, the collective studies of dinuclear transition metal complexes as antitumor agents is a topic worthy of scientific investigation. Attempts

to develop transition metal complexes with greater potency and reduced toxicity has led researchers into the studies of dinuclear metal complexes. Consideration of the currently accepted mechanism of action of cisplatin as well as structure-activity requirements are used as the basis for the search for new and improved transition metal complexes in the fight against cancer and other illnesses.

## **Chapter II**

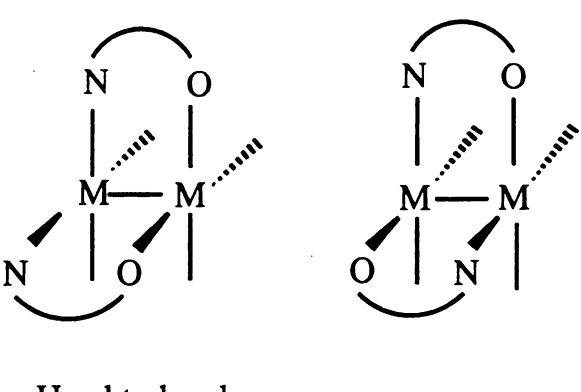
**Dirhodium Anticancer Agents** 

### 1. Introduction

The discovery of the inhibition of DNA replication by dirhodium(II) μ-tetra-carboxylates led us to investigate their interactions with 9ethylguanine (9-EtGH) in hopes of developing model compounds that would lend insight into the process. 19 Previous research efforts did not elucidate the exact binding site of the dirhodium compounds in tumor cell DNA, but studies indicated that covalent interactions with single-stranded or unwound DNA was a likely mode of action.<sup>21</sup> Work in our laboratories established the remarkable finding that the \(\mu\)-tetra-carboxylates of dirhodium(II) form products with two bridging 9-EtGH ligands cis to each other, contrary to previous investigations which suggested that no significant binding occurred between this purine and the dinuclear metal center.<sup>21</sup> It was further discovered that the complexes formed by 9-EtGH,  $[Rh_2(\mu-9-EtGH)_2(\mu-O_2CCH_3)_2((CH_3)_2CO)_2]^{2+}$ , and  $Rh_2(\mu-9-EtG)_2(\mu-O_2CCH_3)_2((CH_3)_2CO)_2$ O<sub>2</sub>CCH<sub>3</sub>)<sub>2</sub>(CH<sub>3</sub>OH)<sub>2</sub> exhibit both "head-to-head" and "head-to-tail" isomers (Figure 8). 19 Since the bases in any given strand of DNA are stacked in a "head-to-head" fashion, the "head-to-head" isomers are the primary targets as model compounds in the context of the mechanism of metal complex attack on DNA. Inter-strand "head-to-tail" products are also possible with these dinuclear metal systems, but this type of bridging in the double helix would most likely create large distortions that are recognized as damaged by DNA repair enzymes and are therefore repaired.

Figure 8

#### Geometrical Isomers



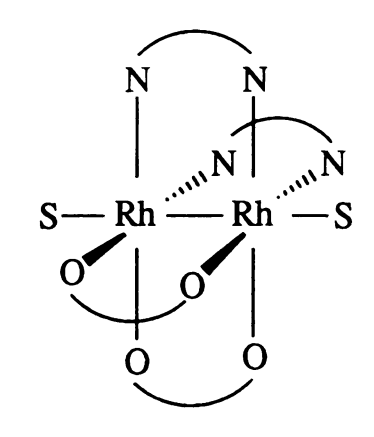
Head to head

Head to tail

Formation of a product containing a bridging 9-EtGH ligand relies on the lability of the equatorial ligands in the lantern structure. One such lantern structure of dinuclear rhodium(II) that strongly retains two of its ligands in a *cis* configuration as well as possessing two labile equatorial ligands is the complex first synthesized by Piraino and co-workers, Rh<sub>2</sub>(μ-DToIF)<sub>2</sub>(μ-O<sub>2</sub>CCF<sub>3</sub>)<sub>2</sub>(H<sub>2</sub>O)<sub>2</sub> (DToIF = N,N'-p-tolylformamidinate) (Figure 9). As compared to μ-tetrakisformamidinate derivatives, *e.g.* Rh<sub>2</sub>(μ-DToIF)<sub>4</sub>, which do not allow access to the equatorial positions, the mixed-ligand derivative exhibits both axial (two) and equatorial (four) coordination sites for binding to Lewis bases. The antitumor activity of this complex was tested against various tumor cell lines and it was found to exhibit equal antitumor activity and a lower toxicity than dinuclear rhodium(II) complexes of the type Rh<sub>2</sub>(μ-O<sub>2</sub>CR)<sub>4</sub>L<sub>2</sub>. The researchers postulate that the lability of the bridging trifluoroacetates and the axial water molecules in solution lead to the formation of the charged solvated

cation,  $[Rh_2(\mu-DTolF)_2S_6]^{2+}$  (S = solvent) which is suspected to be the important physiological form of the active compound.<sup>22</sup>

Figure 9



$$\begin{array}{c}
H_3C \\
N = C \\
N = N
\end{array}$$

S = donor solvent

Although their preliminary work did not include verification of structures by X-ray crystallography, Piraino concluded that adenine and N6,N6-dimethyladenine did not effect the substitution of the equatorial (CF<sub>3</sub>CO<sub>2</sub>)- groups, but instead were axially coordinated through the N3 positions. It was further suggested that the N9 position participates in

hydrogen bonding with an oxygen atom of the equatorial trifluoroacetate groups (Figure 10). It is important to point out that the coordination mode

Proposed structure of  $Rh_2(\mu-DTolF)_2(\mu-O_2CCF_3)_2(ade)_{n,n-1}$ n=2

of the more biologically relevant adenosine is required to be different than that of adenine, since the N3 position in adenosine is sterically hindered from coordination by the ribose ring. Conductivity measurements as well as  $^1H$ -NMR and EPR spectroscopies support the formulation of the adenosine product as the mixed-valence complex,  $[Rh_2(\mu-DTolF)_2(\mu-ado)_2(O_2CCF_3)](O_2CCF_3)$  (where ado = adenosine), with bridging adenosine moieties. The presence of the strongly basic formamidinate groups lowers the oxidation potential of the  $Rh_2^{4+}$  fragment, thereby allowing for the facile formation of mixed valence  $Rh_2^{5+}$  complexes. It was proposed that the purine binds to the  $Rh_2$  core through the N1 and deprotonated N6 positions rather than via the usual N6-N7 positions (Figure 11).

Figure 11

Proposed structure of  $Rh_2(\mu\text{-DTolF})_2(\mu\text{-O}_2CCF_3)_2(A)_{n,n-1}$ A = adenosine; n = 2

Similar results with cytosine, 1-methylcytosine and deoxycytidine derivatives were obtained, but no X-ray structures were determined. Unlike the μ-tetracarboxylate derivatives that are reported to be unreactive towards cytosine, the mixed-ligand complex is described as containing the pyrimidine bound through the N3 and deprotonated exocyclic N4 positions. In addition, Piraino reports that Rh<sub>2</sub>(μ-DTolF)<sub>2</sub>(μ-O<sub>2</sub>CCF<sub>3</sub>)<sub>2</sub>(H<sub>2</sub>O)<sub>2</sub> does not react with guanine, deoxyguanosine and uracil.<sup>22a</sup> This chapter reports complementary work carried out in our laboratories regarding the reactivity of this dinuclear complex with guanine and its substituted derivatives. Along with these results are reported the synthesis, structural

characterization and similar reactions of the novel, partially solvated complex  $[Rh_2(\mu-DTolF)_2(CH_3CN)_6](BF_4)_2$ .

### 2. Experimental

### A. Synthesis

Unless otherwise stated, all reactions were carried out under an argon atmosphere by the use of standard Schlenk-line techniques. The mixed ligand complexes,  $[Rh(cod)(form)]_2$  and  $Rh_2(\mu-form)_2(\mu-O_2CCF_3)_2(H_2O)_2$  (form = N,N'-p-tolylformamidinate, DTolF-; N,N'-diphenylformamidinate, DPhF-), were prepared as described in the literature.<sup>22d</sup> The purine derivatives 9-EtGH and guanosine were purchased from Sigma and were used without further purification.

### Preparation of $Rh_2(\mu-DTolF)_2(\mu-9-EtGH)_2(O_2CCF_3)_2$ (1)

An amount of Rh<sub>2</sub>( $\mu$ -DTolF)<sub>2</sub>( $\mu$ -O<sub>2</sub>CCF<sub>3</sub>)<sub>2</sub>(H<sub>2</sub>O)<sub>2</sub> ( 26 mg, 3.61 x 10<sup>-5</sup> mol) was dissolved in 4 mL of CH<sub>3</sub>CN and 9-EtGH (12.7 mg, 7.08 x 10<sup>-5</sup> mol) was added to the red solution, after which time the mixture was refluxed for approximately 1 h. The olive-green reaction mixture was allowed to cool to room temperature, filtered and treated with Et<sub>2</sub>O to effect precipitation of the product. The green solid was washed with 20 mL of Et<sub>2</sub>O and dried under reduced pressure (32 mg, 83% yield). <sup>1</sup>H NMR (CD<sub>3</sub>CN)  $\delta$  ppm: 1.35-1.37 (m, CH<sub>3</sub>), 1.95 (s, CH<sub>3</sub>CN), 2.15 broad (s, H<sub>2</sub>O), 2.23 (s, CH<sub>3</sub>), 4.05 (m, CH<sub>2</sub>), 6.80 (d, phenyl), 6.89 (d, phenyl), 7.03-7.19 broad (m, phenyl), 7.55 (m, NCHN), 7.99 (s, H8), 8.02 (s, H8). <sup>19</sup>F NMR (both CD<sub>3</sub>CN and acetone-d6)  $\delta$  ppm: <sup>-</sup>12.49 referenced to C<sub>6</sub>H<sub>5</sub>CF<sub>3</sub> (s, O<sub>2</sub>CCF<sub>3</sub>). IR (Nujol, NaCl) cm<sup>-1</sup> 1647 mb, 1564 s, 1487 s, 1360 m, 1261 s, 1199 s, 1134 br, 1084 br, 1028 br.

### Preparation of $Rh_2(\mu-DPhF)_2(\mu-9-EtGH)_2(O_2CCF_3)_2$ (2)

Rh<sub>2</sub>( $\mu$ -DPhF)<sub>2</sub>( $\mu$ -O<sub>2</sub>CCF<sub>3</sub>)<sub>2</sub>(H<sub>2</sub>O)<sub>2</sub> (16.8 mg, 2.34 x 10<sup>-5</sup> mol) was dissolved in 5 mL of distilled CH<sub>3</sub>CN and 9-EtGH (9.0 mg, 5.0 x 10<sup>-5</sup> mol) was added to the red solution. After ~1 h of constant reflux the solvent was evaporated under reduced pressure to yield a dark green residue which was dried and redissolved in acetone (~3 mL). The green acetone solution was treated with ~5 mL of hexanes and cooled to ~-10 °C. The bright green precipitate was removed by filtration and dried *in vacuo* (19 mg, 79% yield). <sup>1</sup>H NMR (CD<sub>3</sub>CN)  $\delta$  ppm: 1.35-1.38 (m, CH<sub>3</sub>), 1.95 (s, CH<sub>3</sub>CN), 2.21 broad (s, H<sub>2</sub>O), 4.04-4.07 broad (m, CH<sub>2</sub>), 6.82 (d, phenyl), 6.89 (d, phenyl), 7.04-7.20 broad (m, phenyl), 7.55 (m, NCHN), 7.93 (s, H8), 8.03 (s, H8). <sup>19</sup>F NMR (both CD<sub>3</sub>CN, acetone-d6)  $\delta$  ppm: -12.47 referenced to C<sub>6</sub>H<sub>5</sub>CF<sub>3</sub> (s, O<sub>2</sub>CCF<sub>3</sub>). <sup>103</sup>Rh NMR (CD<sub>3</sub>CN)  $\delta$  ppm: 5551.98.

### Preparation of $[Rh_2(\mu-DTolF)_2(CH_3CN)_6](BF_4)_2$ (3)

A quantity of [Rh(cod)(DTolF)]<sub>2</sub> (97 mg, 1.50 x 10<sup>-4</sup> mol) and AgBF<sub>4</sub> (120 mg, 6.16 x 10<sup>-4</sup> mol) was dissolved in 20 mL of a 1:1 mixture of CH<sub>2</sub>Cl<sub>2</sub> and CH<sub>3</sub>CN in the absence of light. After 2-3 h the yellow-orange mixture had changed to a clear, pale green solution. The mixture was stirred for an additional 2 days during which time silver metal was observed to precipitate. The mixture was filtered through a Celite plug, and the orange-red filtrate was concentrated under reduced pressure. Following the addition of 3 mL of Et<sub>2</sub>O, the mixture was cooled to ~10 °C. An orange-red microcrystalline precipitate was collected by filtration, washed with 3 x 5 mL Et<sub>2</sub>O and dried *in vacuo* (138 mg, 93% yield). <sup>1</sup>H NMR (CD<sub>3</sub>CN) δ ppm: 1.96 (s, CH<sub>3</sub>CN), 2.25 (s, CH<sub>3</sub>), 2.49 (s, CH<sub>3</sub>CN), 6.99 (m, phenyl), 7.51 (t, NCHN). <sup>103</sup>Rh NMR (CD<sub>3</sub>CN) δ ppm: 4648.73.

### Preparation of $[Rh_2(\mu-DTolF)_2(\mu-9-EtGH)_2(CH_3CN)_2](BF_4)_2$ (4)

- (a) A quantity of 9-ethylguanine (41.7 mg, 0.233 mmol) was added to a stirring solution of  $[Rh_2(\mu-DTolF)_2(CH_3CN)_6](BF_4)_2$  (115.4 mg, 0.116 mmol) dissolved in of 5 mL of CH<sub>3</sub>OH and 10 mL of CH<sub>3</sub>CN. The mixture was gently refluxed for ~2 h, during which time the orange-red mixture with the suspended 9-ethylguanine became a clear green solution. The reaction mixture was filtered, and the filtrate was evaporated *in vacuo* to yield a green solid (60 mg, 47% yield). <sup>1</sup>H NMR (CD<sub>3</sub>OD)  $\delta$  ppm: 1.36 (t, CH<sub>3</sub>), 1.40 (t, CH<sub>3</sub>), 1.92 (s, CH<sub>3</sub>CN), 2.23 (s, CH<sub>3</sub>), 3.98 (q, CH<sub>2</sub>), 4.05 (q, CH<sub>2</sub>), 6.80 (m, phenyl), 6.89 (m, phenyl), 7.00 (m, phenyl), 7.50 (t, NCHN), 7.55 (t, NCHN), 8.32 (s, H8), 8.35 (s, H8). IR (Nujol, NaCl) cm<sup>-1</sup> 2311 s, 2305 s, 1641 m,br, 1608 m, 1577 s, 1508 s, 1027 s, 1178 s, 1057 br, 821 s, 790 s, 763 s, 721 s.
- (b) The above reaction was repeated with an acetonitrile and acetone solvent mixture. Two equivalents of 9-EtGH (46 mg, 2.57 x 10<sup>-4</sup> mol) were added to a stirring acetonitrile (5 mL) and acetone mixture (1 mL) of (4) (138.5 mg, 1.29 x 10<sup>-4</sup> mol), and the mixture was stirred at constant reflux for ~3 h. The reaction mixture was filtered in air through a Celite plug and the solvent was removed *in vacuo* (110 mg, 78 % yield).

### Synthesis of $[Rh_2(\mu-DTolF)_2(\mu-9-EtGH)_2(CH_3CN)_2](BPh_4)_2$ (5)

The metathesis of (4a) with two equivalents of AgBPh<sub>4</sub> in acetone yields (5) in nearly quantitative yields. IR (Nujol, NaCl) cm<sup>-1</sup> 1585 b, 1504 s, 1261 s, 1084 m,br, 1028 s, 804 m.

### B. X-ray Crystallography

The structure of  $[Rh_2(\mu-DTolF)_2(CH_3CN)_6](BF_4)_2$  (3) was determined by the application of general procedures that have been fully described elsewhere.<sup>24</sup> Geometric and intensity data were collected on a

Rigaku AFC6S diffractometer with graphite-monochromated MoK $\alpha$  ( $\lambda_{\alpha}$  = 0.71069 Å) radiation and were corrected for Lorentz and polarization effects. A unit cell for [Rh<sub>2</sub>( $\mu$ -DTolF)<sub>2</sub>( $\mu$ -9-EtGH)<sub>2</sub>(CH<sub>3</sub>CN)<sub>2</sub>](BF<sub>4</sub>)<sub>2</sub> (4) was determined on a Nicolet P3/V diffractometer upgraded to a Siemens P3/F with graphite monochromated MoK $\alpha$  ( $\lambda_{\alpha}$  = 0.71073 Å) radiation; the reflections were corrected for Lorentz and polarization effects. All calculations were performed with VAX computers on a cluster network within the Department of Chemistry at Michigan State University using the Texsan software package of the Molecular Structure Corporation. <sup>23</sup> [Rh<sub>2</sub>( $\mu$ -DTolF)<sub>2</sub>(CH<sub>3</sub>CN)<sub>6</sub>](BF<sub>4</sub>)<sub>2</sub> (3)

(i) Data Collection and Reduction. Large single crystals of (2) were obtained from the slow diffusion of a concentrated acetonitrile solution into toluene. The crystals grew as long orange-red crystals at the interface of the two solvents after 12 days. A suitable single crystal, with the approximate dimensions of 0.78 x 0.26 x 0.21 mm<sup>3</sup>, was mounted on the tip of a glass fiber with Dow Corning grease. Cell constants were obtained from a least squares refinement using 24 carefully centered reflections in the range  $29^{\circ} < 2\theta < 37^{\circ}$ . Data were collected at  $^{-}100 \pm 1$  °C in the range  $4 \le 2\theta \le 47^{\circ}$ , by using the  $\omega$ -scan method. Weak reflections (those with F  $< 10\sigma(F)$ ) were rescanned at a maximum of 3 rescans and the counts were accumulated to ensure good counting statistics. A total of 8005 reflections were collected; of these 3865 reflections with  $F_0^2 > 3\sigma(F_0)^2$  were used in the measurement. Periodic measurement of three representative reflections at regular intervals revealed that no loss of diffraction intensity had occurred during data collection. An empirical absorption correction was applied on the basis of azimuthal scans of 3 reflections with  $\gamma$  near 90°.

(ii) Structure Solution and Refinement. The space group was determined to be Pbca based on the observed systematic absences. The positions of all non-hydrogen atoms were obtained by application of the direct methods programs MITHRIL and DIRDIF followed by successive full-matrix least-squares cycles.<sup>24</sup> All non-hydrogen atoms were refined with anisotropic thermal parameters. Hydrogen atoms were treated as fixed contributors at idealized positions and were not refined. Final least squares refinement of 567 parameters resulted in residuals of R = 0.046 and  $R_w = 0.063$  and a goodness-of-fit = 2.01. A final difference Fourier map revealed the highest peak in the difference map to be  $0.87 \text{ e}^{-}/\text{Å}^3$ .

# $[Rh_2(\mu-DTolF)_2(\mu-9-EtGH)_2(CH_3CN)_2](BF_4)_2$ (4)

(i) Cell Determination. Single crystals of (4) were obtained from slow diffusion of a concentrated CH<sub>3</sub>OH solution of the compound into toluene. The crystals grew as prismatic rectangles over a period of 3-4 weeks. A single crystal was mounted on the tip of a glass fiber with Dow Corning grease. Geometric and intensity data were collected at  $^{-1}00 \pm 2$  °C. Indexing and refinement of 15 reflections in the range  $4 \le 20 \le 12^{\circ}$  selected from a rotational photograph gave preliminary unit cell parameters for an orthorhombic C-centered crystal system.

### C. <sup>103</sup>Rh NMR Spectroscopy

The  $^{103}$ Rh NMR spectra were recorded on a Varian 500-MHz spectrometer equipped with a 5 mm Nalorac  $^{103}$ Rh probe with an acquisition time of 12-16 h. The pulse width was 10  $\mu$ s at a temperature of  $^{\sim}35$  °C.  $^{103}$ Rh NMR shifts are referenced to  $[\Xi](^{103}$ Rh) = 3.16 MHz (Equation 1). $^{25}$  The term  $\delta$  is the chemical shift,  $\delta$ ' is chemical shift with respect to the published reference (TMS),  $\Xi$  is the frequency of the desired reference ( $^{103}$ Rh),  $\Xi$ ' is the frequency of the published reference.

### Equation 1

$$\delta = \delta'(\Xi'_{ref}/\Xi_{ref}) + [(\Xi'_{ref}-\Xi_{ref})/\Xi_{ref}] \times 10^6$$

#### 3. Results

### A. Spectroscopic Properties of (1) and (2)

The solid-state structures of  $Rh_2(\mu-form)_2(\mu-O_2CCF_3)_2(H_2O)_2$  complexes lend insight into the possible structures of (1) and (2).  $Rh_2(\mu-form)_2(\mu-O_2CCF_3)_2(H_2O)_2$  exhibits two *cis-DTolF* and two *cis-O\_2CCF\_3* groups spanning the metal centers. Equatorial substitution of the  $(CF_3CO_2)^-$  ligands is expected due to the weak binding interactions of these ligands in comparison to the basic formamidinate ligands. Drawings of the proposed structures for (1) and (2) (including different isomers) are depicted in Figure 12.

The characterization of dinuclear metal centers ligated by purines by  $^{1}$ H NMR spectroscopy is useful because of the characteristic downfield shift of the H8 signal by 0.5 to 1 ppm ( $\delta$  = 7.63 ppm for free 9-EtGH in CD<sub>3</sub>OD).<sup>4</sup> The  $^{1}$ H NMR spectra of (1) and (2) exhibit two signals assignable to the H8 positions of bridging 9-ethylguanines with H8 shifts observed at a  $\delta$  > 7.9 ppm (Figure 13). The presence of signals attributable to 9-EtGH in CD<sub>3</sub>CN is an important observation since the purine is insoluble in this solvent.

Another important point that should be addressed is the color change that occurs during the reaction. The parent dirhodium(II) complexes, Rh<sub>2</sub>(μ-form)<sub>2</sub>(μ-O<sub>2</sub>CCF<sub>3</sub>)<sub>2</sub>(H<sub>2</sub>O)<sub>2</sub>, are green solids that yield red solutions upon addition of CH<sub>3</sub>CN which displaces the axial water molecules. Green colors for dirhodium(II) complexes are usually associated with axial

oxygen donors, while red colors are associated with axial nitrogen donors. The color change back to green that occurs with coordination of 9-EtGH is attributed to the presence of an oxygen atom from CF<sub>3</sub>CO<sub>2</sub>- ligands bound to the axial positions.

The two H8 signals observed in the spectra for (1) and (2) indicate the presence of two isomers in a roughly 1:1 ratio, based on integration. The two isomers are proposed as being the polar "head-to-head" and less polar "head-to-tail" isomers (Figure 8). One would expect the less polar isomer to be of lower energy than the "head-to-head" isomer by analogy to complexes of the type  $M_2(x-hp)_4$  (x-hp = 6-substituted hydroxypyridine) where the non-polar isomers are preferred over the polar ones.<sup>26</sup> The presence of both isomers in the <sup>1</sup>H NMR spectrum indicates a small energy difference in the formation of the two compounds.

The previously characterized products of reactions between  $Rh_2(O_2CR)_4L_2$  and 9-EtGH have demonstrated that two types of bridging guanine ligands are possible: (i) 9-EtGH, the neutral ligand form and (ii) 9-EtG- the anionic or deprotonated form, where the purine is deprotonated at the N1 position (Figure 14). It has been documented that the  $pK_a$  of the N1 position is lowered by 1.5-2.0  $pK_a$  units upon coordination to platinum complexes (from ~9.4 to 8.0).<sup>7</sup> The anionic ligand, 9-EtG- has also been observed to form *in situ* in acidic media.<sup>7</sup> The deprotonation of N1-H in guanine is observed in reactions with metal complexes containing basic leaving groups such as  $CH_3CO_2$ - ( $pK_b = 9.25$ ). The much lower basicity of the trifluoroacetate leaving groups of (1) and (2) ( $pK_b > 13$ ) are expected to allow the coordination of the neutral 9-EtGH species to the dinuclear metal center.

Figure 12

head-to-head isomer

head-to-tail isomer

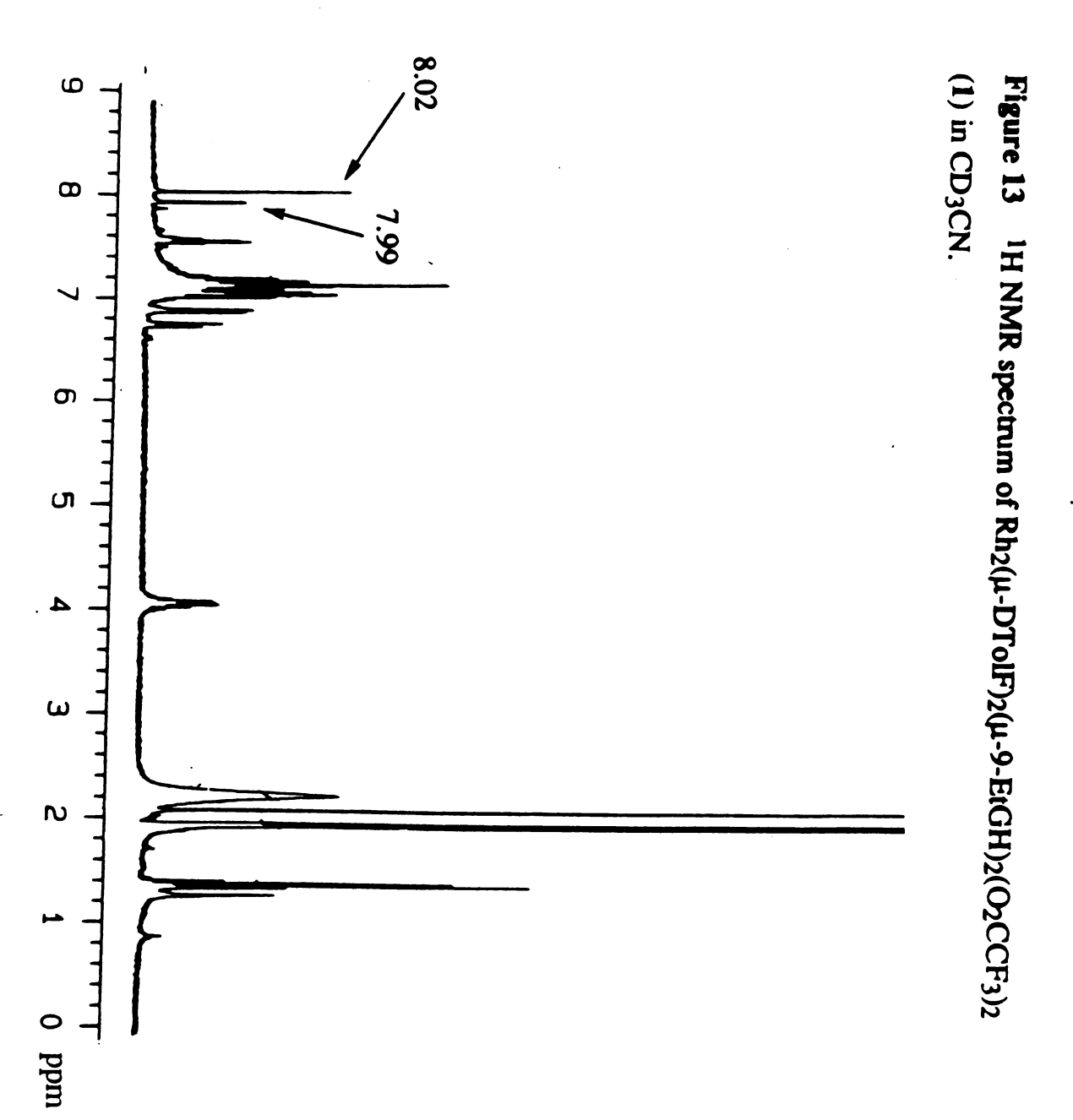


### Figure 14

$$H_{2N} \xrightarrow{N} N \xrightarrow{pK_{a} \sim 3} N \xrightarrow{pK_{a} \sim 3} N \xrightarrow{N} N \xrightarrow{N} N$$

neutral guanine

N1 deprotonated guanine

The green color of compounds (1) and (2) supports the presence of axial CF<sub>3</sub>CO<sub>2</sub>- groups in the solid state.<sup>26</sup> The <sup>19</sup>F NMR spectra of complexes (1) and (2) (-12.49 and -12.47 ppm, respectively) are indicative of dissociated CF<sub>3</sub>CO<sub>2</sub>- groups in solution.<sup>27</sup> <sup>19</sup>F NMR signals for bridging equatorial CF<sub>3</sub>CO<sub>2</sub>- groups are commonly observed 50-60 ppm upfield ( $\delta \sim -77$  ppm) from the free acid referenced to C<sub>6</sub>H<sub>5</sub>CF<sub>3</sub>. Axially coordinated CF<sub>3</sub>CO<sub>2</sub>- groups have been observed approximately in the same region.<sup>27</sup> The singlets at -12.49 ppm for (1) and -12.47 ppm for (2) are indicative of outer-sphere CF<sub>3</sub>CO<sub>2</sub>. Displacement of these groups by acetonitrile is conceivable, but solvent displacement by a weak donating solvent like acetone (the solvent used for the <sup>19</sup>F NMR experiment) is The observed signal indicates the relatively weak binding strength of the trifluoroacetate ligand to the [Rh<sub>2</sub>(form)<sub>2</sub>]<sup>2+</sup> species in Similar <sup>19</sup>F NMR spectra are observed for the starting solution. compounds  $Rh_2(\mu\text{-form})_2(\mu\text{-O}_2CCF_3)_2(H_2O)_2$  which support a rapid exchange of the labile equatorial ligands at room temperature. extreme lability of the CF<sub>3</sub>CO<sub>2</sub>- ligands can be explained by the strong σdonation of the formamidinate ligands which weaken the equatorial Rh-O interactions. The inductive and resonance effects from the tolyl groups that are *trans* to the CF<sub>3</sub>CO<sub>2</sub>- groups donate electron density to the N atoms, which in turn direct the added electron density toward the dinuclear center, thereby weakening the CF<sub>3</sub>CO<sub>2</sub>- binding interactions.

### B. Spectroscopic and Crystallographic Properties of (3)

The novel, partially solvated complex, (3) was prepared after our discovery of the related complex,  $Ir_2(\mu$ recent  $DTolF_{2}(CH_{3}CN)_{6}](BF_{4})_{2}.^{28}$  Early studies of  $Rh_{2}(\mu-DTolF)_{2}(\mu-DTolF)_{3}$ O<sub>2</sub>CCF<sub>3</sub>)<sub>2</sub>(H<sub>2</sub>O)<sub>2</sub> suggested the formation of the solvated species in solution with trifluoroacetate being liberated as an anion.<sup>22b</sup> We hoped that slight variations such as replacing the counterions would increase the chances of obtaining single crystals suitable for X-ray diffraction studies. The labile acetonitrile ligands in (3) render this complex ideal for the synthesis of other interesting  $[Rh_2(\mu\text{-form})_2]^{2+}$  derivatives that are not available by other routes. Crystal parameters and basic information pertaining to data collection are summarized in Table 2. The ORTEP representation of (3) is depicted in Figure 15, and bond distances and angles are presented in Table 3. From this information, insight into the structures of  $[Rh_2(\mu\text{-form})_2(\mu\text{-9-EtGH})_2]^{2+}$  moieties may be gained.

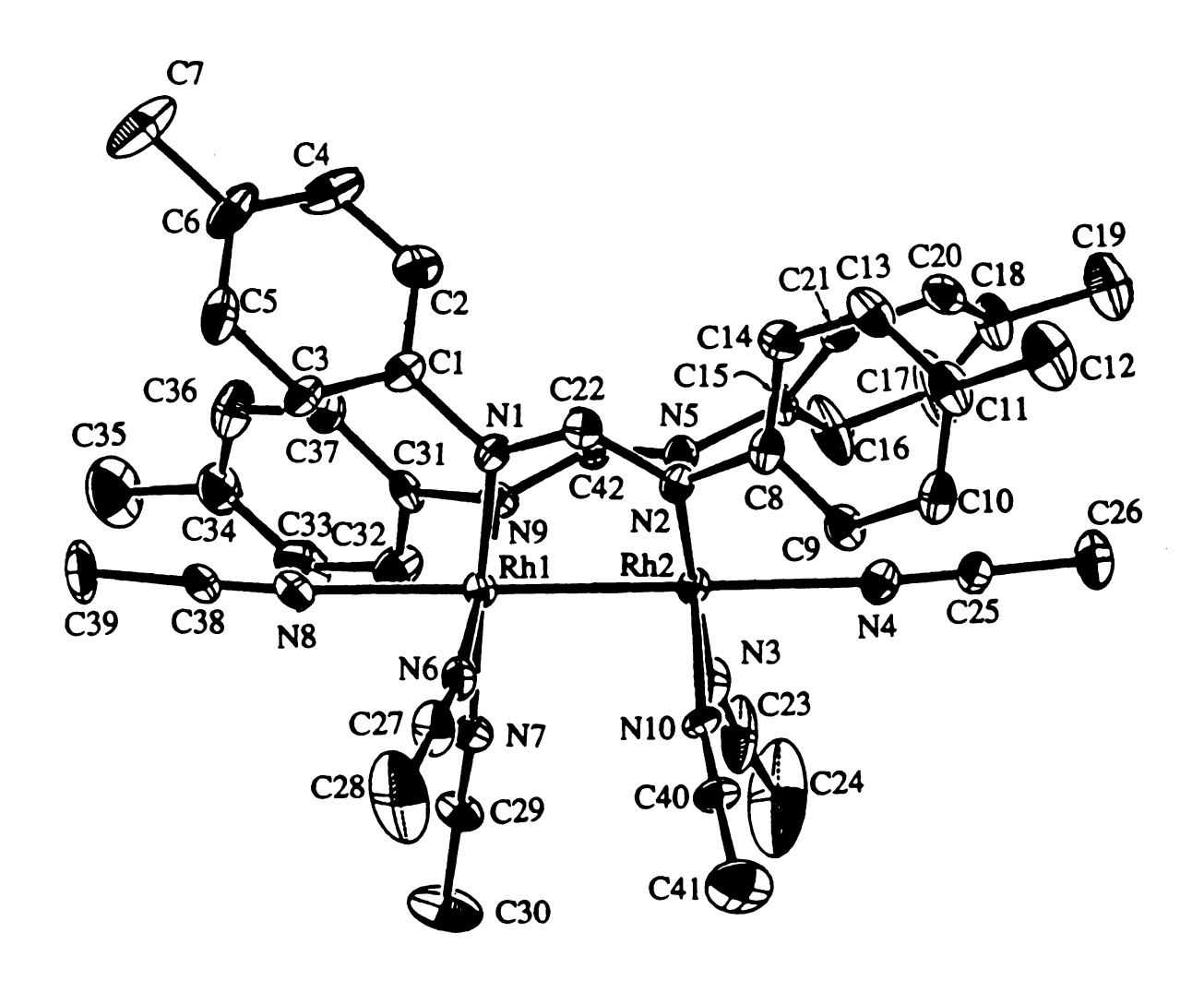
Compound (3) crystallizes in an orthorhombic-C crystal system. The equatorial bridging DTolF- groups are cis to each other with average torsional twist angles of 18° (Table 4). This degree of non-ideality for the Rh<sub>2</sub><sup>4+</sup> moiety is not uncommon and is observed with most of the metalmetal single bonded structures of this type.<sup>26</sup> The angles formed by the N-C-N fragments contained in the five-membered ring (123 (1)° and 124 (1)°) are within normal ranges observed for similar compounds. The C-N distances of the formamidinate fragments (~1.33 (1) Å) are sufficiently short so as to suggest significant double bond character for the N-C-N

groups. The Rh-N (~2.04 (9) Å) bond distances to the formamidinate groups are longer than the corresponding distances in the *bis*-trifluoroacetate derivative (1.99 (4) Å). The average equatorial acetonitrile M-N distance is approximately 0.04 Å shorter than the metal-formamidinate distances, supporting a strong  $\sigma$ -donation to the dinuclear center. The axial acetonitrile interactions, Rh1-N8 (2.188 (8) Å) and Rh2-N4 (2.211 (8) Å), are ~0.1 Å shorter than the axial acetonitrile interaction observed in the crystal structure of the *tetra*-formamidinate derivative, Rh<sub>2</sub>( $\mu$ -DPhF)<sub>4</sub>(NCCH<sub>3</sub>) (2.106(4) Å). This implies the presence of fairly weak axial interactions.<sup>5</sup>

The Rh-Rh bond distance of (3), 2.560(1) Å, is slightly longer than that found in *cis*-Rh<sub>2</sub>(μ-DTolF)<sub>2</sub>(μ-O<sub>2</sub>CCF<sub>3</sub>)<sub>2</sub>(H<sub>2</sub>O)<sub>2</sub>, which exhibits a Rh-Rh bond distance of 2.43(1) Å.<sup>22</sup> The nitrile ligands appear to be stronger electron donors than the trifluoroacetate ligands based on <sup>103</sup>Rh NMR chemical shifts. It is difficult to ascertain whether the addition of a bridging unit such as 9-EtGH will lengthen or shorten the Rh-Rh bond compared to the trifluoroacetate derviative, but it is safe to assume that the electron donation from the neutral purine would allow for similar metalmetal bonding.

A <sup>1</sup>H NMR spectrum of (3) is in accord with the structural data from the crystallographic results. The singlet at  $\delta = 1.96$  ppm is assignable to the axial acetonitrile ligands whereas the singlet at  $\delta = 2.49$  ppm can be attributed to the equatorial acetonitrile groups. The singlet at  $\delta = 2.25$  ppm is due to the four equivalent methyl groups of the tolyl substituent, and a multiplet centered at  $\delta \sim 6.9$  ppm is assigned to the phenyl rings. The triplet centered at  $\delta = 7.51$  ppm is observed for the H atom of the N-CH-N fragment of the formamidinate groups with <sup>103</sup>Rh-<sup>1</sup>H coupling of 30 Hz..

Figure 15



ORTEP Representation of [Rh<sub>2</sub>(DTolF)<sub>2</sub>(CH<sub>3</sub>CN)<sub>6</sub>]<sup>2+</sup>.

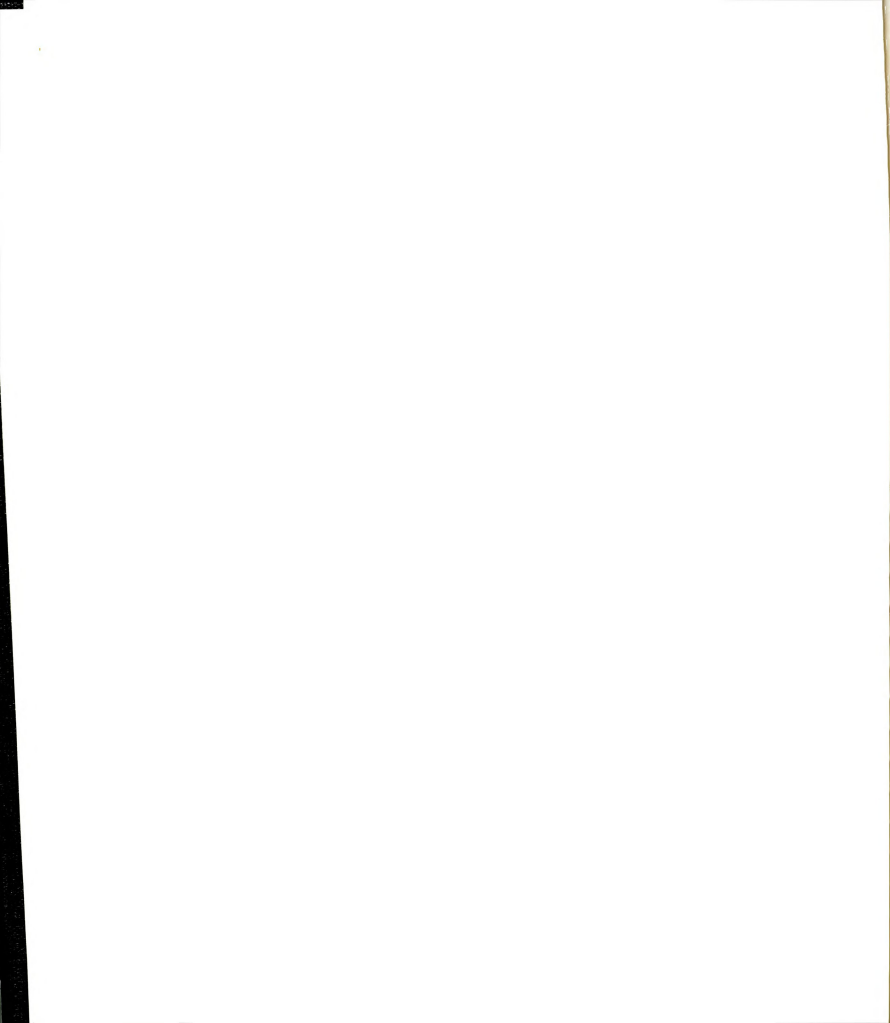
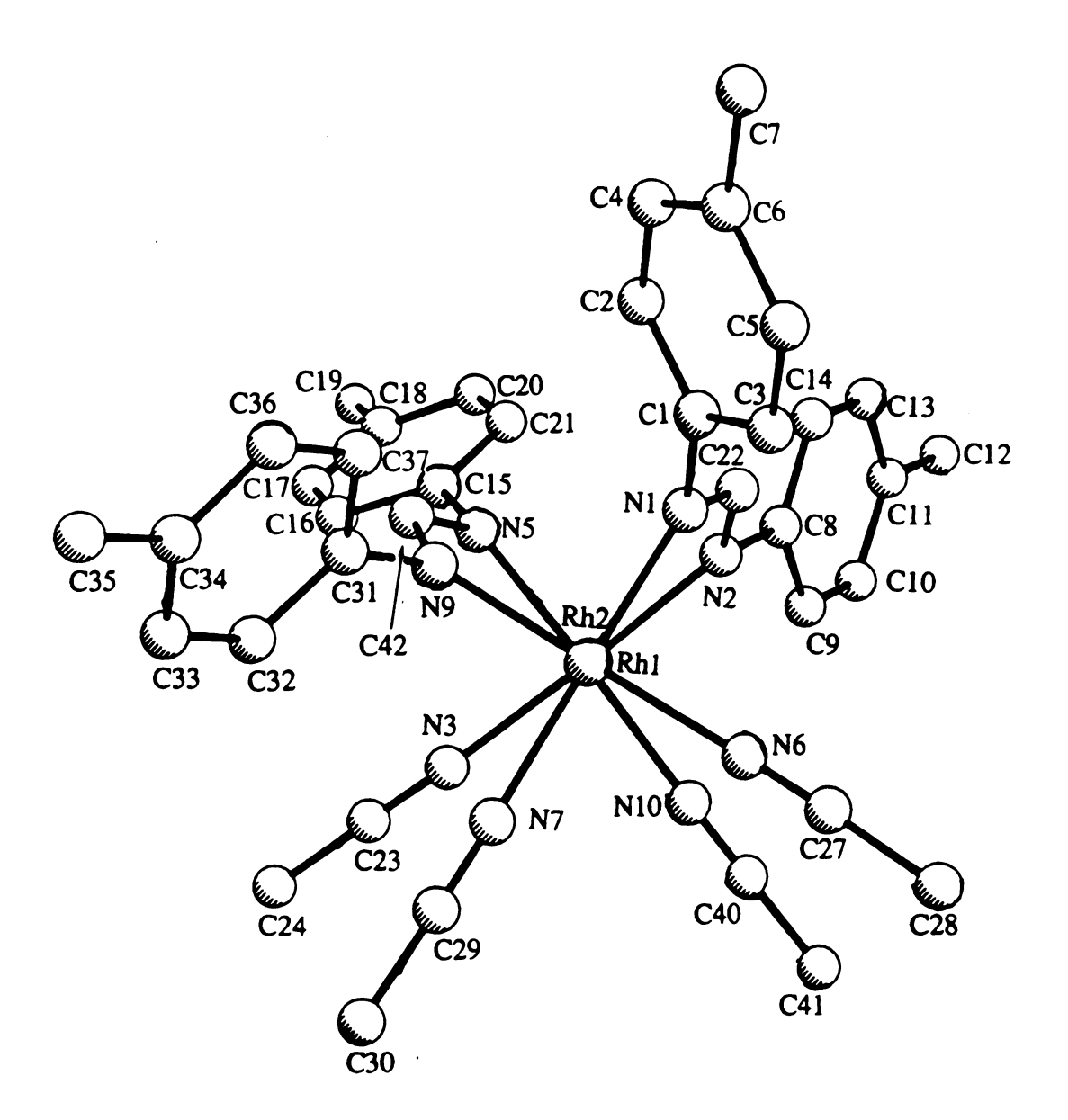


Table 2. Summary of important crystallographic data for [Rh<sub>2</sub>(μ-DTolF)<sub>2</sub>(CH<sub>3</sub>CN)<sub>6</sub>][BF<sub>4</sub>]<sub>2</sub> (3)

formula	Rh <sub>2</sub> C <sub>42</sub> H <sub>60</sub> N <sub>10</sub> B <sub>2</sub> F <sub>8</sub>
formula weight	1084.42
space group	Pbca
a, Å	21.646 (3)
b, Å	31.272 (3)
c, Å	14.561 (4)
α, deg	90
β, deg	90
γ, deg	90
V, Å3	9857 (3)
Z	8
d <sub>calc</sub> , g/cm <sup>3</sup>	1.461
μ (MoKα), cm <sup>-1</sup>	7.27
temp, °C	$-100 \pm 2$
no. of unique reflections	3865
no. of variables	567
reflection/parameter ratio	6.82
Ra	0.046
$R_{\mathbf{w}}^{\mathbf{b}}$	0.063

a R=  $\sum ||F_0| - |F_c||/\sum |F_0|$ . b R<sub>w</sub> =  $[\sum w(|F_0| - |F_c|)^2/\sum w|F_0|^2]^{1/2}$ ; w =  $1/\sigma^2(|F_0|)$ 

Figure 16



PLUTO Representation of [Rh<sub>2</sub>(DTolF)<sub>6</sub>(CH<sub>3</sub>CN)<sub>6</sub>]<sup>2+</sup> Depicting Torsion Angles.



Table 3. Selected bond distances and bond angles for  $[Rh_2(\mu-DTolF)_2(CH_3CN)_6][BF_4]_2$  (3)

# **Bond Distances**

A	В	<b>A-B</b> (Å)	A	В	<b>A-B</b> (Å)
Rh1	Rh2	2.560(1)	Rh1	N1	2.026(8)
Rh1	N6	2.00(1)	Rh1	N7	2.016(9)
Rh1	N8	2.188(8)	Rh1	N9	2.030(8)
Rh2	N2	2.047(8)	Rh2	N3	2.01(1)
Rh2	N4	2.211(8)	Rh2	N5	2.052(8)
Rh2	N10	2.020(9)	N1	C22	1.31(1)
N2	C22	1.33(1)	N5	C42	1.32(1)
N9	C42	1.33(1)			
		Bond	Angles		
A	В		С	A	-B-C (°)
Rh2	Rh	1	N8	17	78.0(3)
N1	Rh	1	N7	17	77.4(4)
N6	Rh	1	<b>N</b> 9	17	78.2(4)
N2	Rh	2	N3	17	77.6(4)
N5	C4:	2	<b>N</b> 9	12	24.0(1)
N1	C2:	2	N2	12	23.0(1)
Rh1	Rh	2	N4	17	76.4(3)
N1	Rh	1	N6	88	3.7(4)
N1	Rh	1	N8	96	5.4(4)
N2	Rh	2	N4	95	5.8(4)
N2	Rh	2	N10	91	5

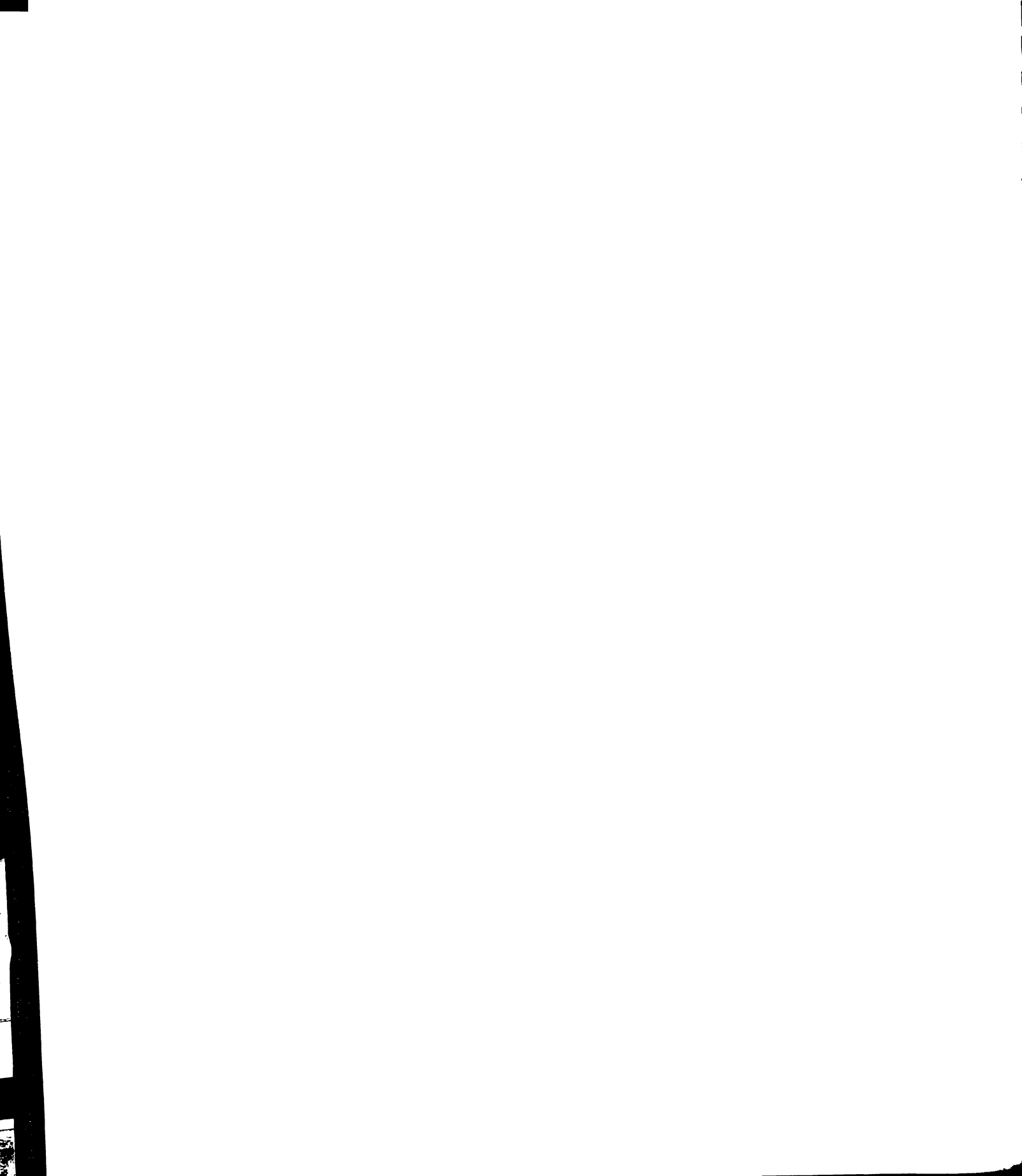
Table 4. Torsion angles of  $[Rh_2(\mu-DTolF)_2(CH_3CN)_6][BF_4]_2$  (3)

A	В	C	D	A-B-C (0)
Rh1	Rh2	N2	C22	-22.9(8)
Rh1	Rh2	N5	C42	-25.3(8)
Rh2	Rh1	N1	C22	-20.7(8)
Rh2	Rh1	N9	C42	-17.9(8)
N1	Rh1	Rh2	N2	18.6(4)
N5	Rh2	Rh1	N9	18.5(4)

### C. Spectroscopic and Crystallographic Properties of (4)

The reaction of (3) with two equivalents of 9-EtGH was carried out in three different solvent systems. The use of CH<sub>3</sub>CN proved to be unsuccessful due to the extreme insolubility of the purine in this solvent. Upon addition of CH<sub>3</sub>OH to the CH<sub>3</sub>CN suspension, however, the reaction mixture became green which signified that a reaction was occurring. Prolonged heating in CH<sub>3</sub>OH should be avoided, as it reduces the dimetal species to rhodium metal, which is not unusual in light of the fact that methanol reduction of Rh<sub>2</sub>(O<sub>2</sub>CCH<sub>3</sub>)<sub>4</sub>(CH<sub>3</sub>OH)<sub>2</sub> occurs readily under conditions of heating.26,29 As found for the products formed from the reaction with the  $\mu$ -tetracarboxylates and 9-EtGH, (4) exhibits two H8 <sup>1</sup>H NMR resonances in a 1:1 ratio both in CD<sub>3</sub>OD and CD<sub>3</sub>CN at  $\delta = 8.32$  and 8.35 ppm (Figure 17). The two triplets observed for the N-CH-N signals at  $\delta = 7.50$  and 7.55 ppm are also a direct indication of two types of formamidinate environments with <sup>103</sup>Rh-<sup>1</sup>H coupling of 30 Hz. The broad resonances in the aromatic region of the formamidinate ligand as well as the broadened ethyl regions of the purine further support this assumption. The spectrum in deuterated methanol reveals a chemical shift for the H8 region of ~0.7 ppm.

Since the two isomers proposed for the structure of (4) differ in polarities, it is conceivable that their solubilities will also differ. A slight variation in solubility was observed when the mixture was subjected to the slow addition of toluene. A <sup>1</sup>H NMR spectrum of the precipitate obtained from the separation exhibited two signals in the H8 region at  $\delta = 8.32$  and 8.35 ppm in a 1:2 ratio, respectively (Figure 17a). The <sup>1</sup>H NMR spectrum of the filtrate reinforced this observation, as two signals in a reverse 2:1 ratio, were observed (Figure 17b).



Single crystals of (4) were obtained by slow diffusion of a concentrated methanol solution layered with toluene at room temperature. Unfortunately, X-ray data collection for this crystal had to be aborted due to instrument failure. The preliminary unit cell for (4) supports the conclusion that it is a new compound. Attempts to reproduce single crystals of (4) are currently underway. The results for the unit cell are presented in Table 5. The isolation of (5) was carried out in an attempt to obtain better quality crystals of [Rh<sub>2</sub>(µ-DTolF)<sub>2</sub>(µ-9-EtGH)<sub>2</sub>L<sub>2</sub>]<sup>2+</sup>. A concentrated solution of (5) in acetone was allowed to slowly diffuse into toluene to afford long green fibers which were deemed unsuitable for single crystal X-ray diffraction. Further anionic substituions are currently underway.

### D. 103Rh NMR Spectroscopy

# 1. Theory of <sup>103</sup>Rh NMR Chemical Shifts

Although  $^{103}$ Rh is 100% abundant,  $^{103}$ Rh NMR spectroscopy is difficult to obtain. The problems arise from the inherent sensitivity of this nucleus, as well as the relatively long spin-lattice relaxation time and very low frequency ( $\Xi = 3.16$  MHz). $^{25a}$ 

 $^{103}$ Rh NMR spectroscopy allows for the direct spectroscopic probing of the local symmetry at the metal center. The chemical shifts of  $^{103}$ Rh nuclei are interpreted in terms of the Ramsey theory of nuclear magnetic shielding. Ramsey's equation is comprised of two parts: (i) the diamagnetic term ( $\sigma_d$ ), produced by the charge distribution or the ground state electron configuration and (ii) the paramagnetic term ( $\sigma_p$ ), produced by the electronic transition of the ground state electrons and the hindrance of this transition caused by other electrons and nuclei in the molecule. Although the diamagnetic term is a dominant factor in determining NMR shifts for

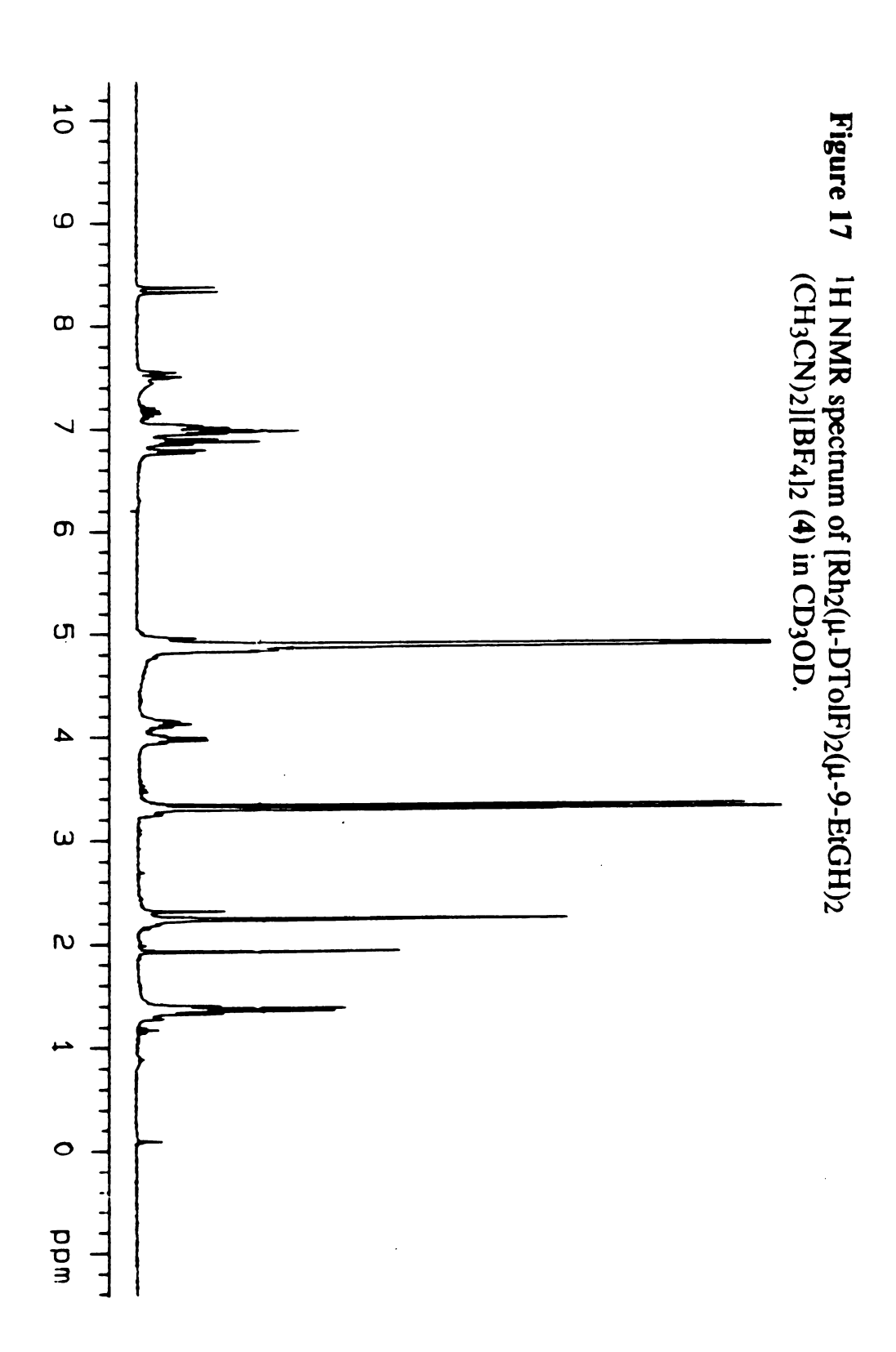
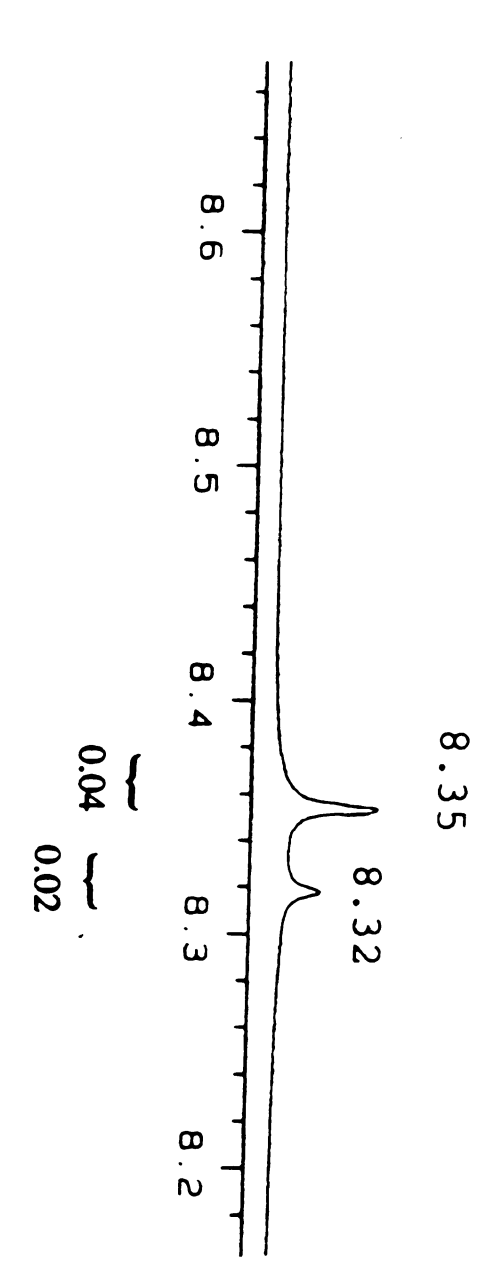
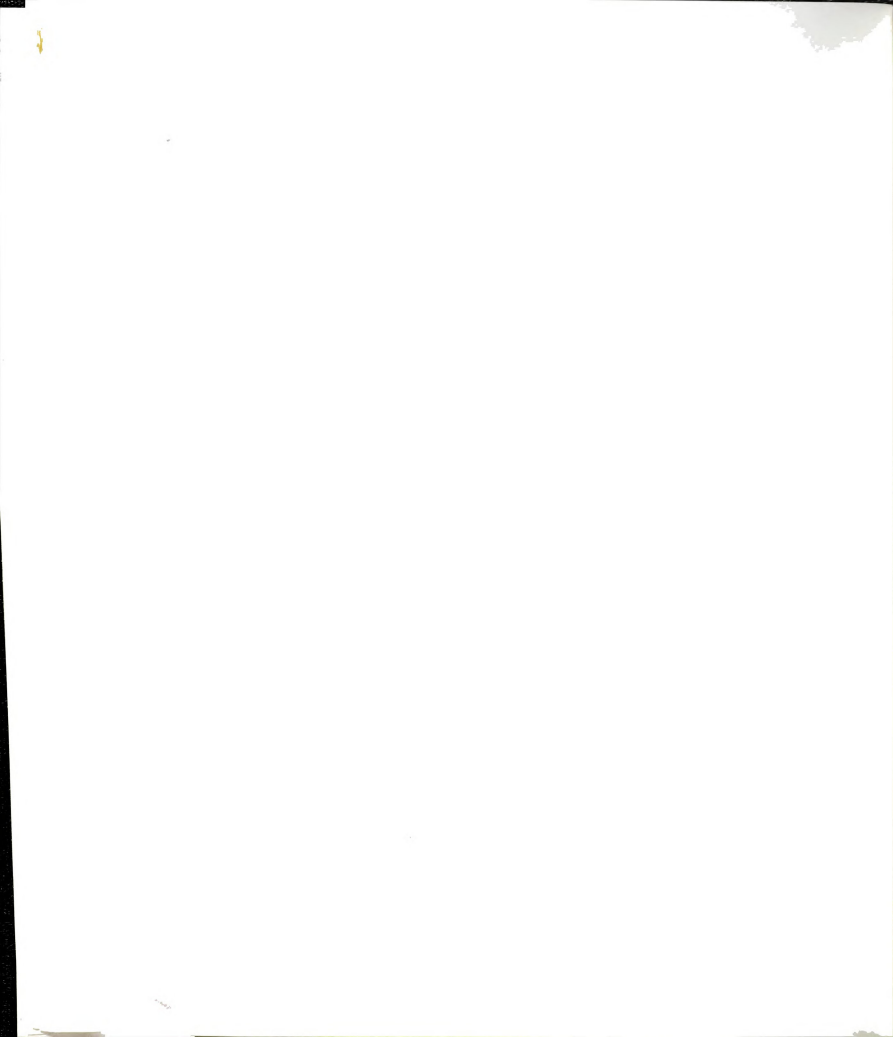


Figure 18 1H NMR spectrum of [Rh<sub>2</sub>(μ-DTolF)<sub>2</sub>(μ-9-EtGH)<sub>2</sub> (CH<sub>3</sub>CN)<sub>2</sub>][BF<sub>4</sub>]<sub>2</sub> (4) in CD<sub>3</sub>OD. Precipitate following the addition of toluene.





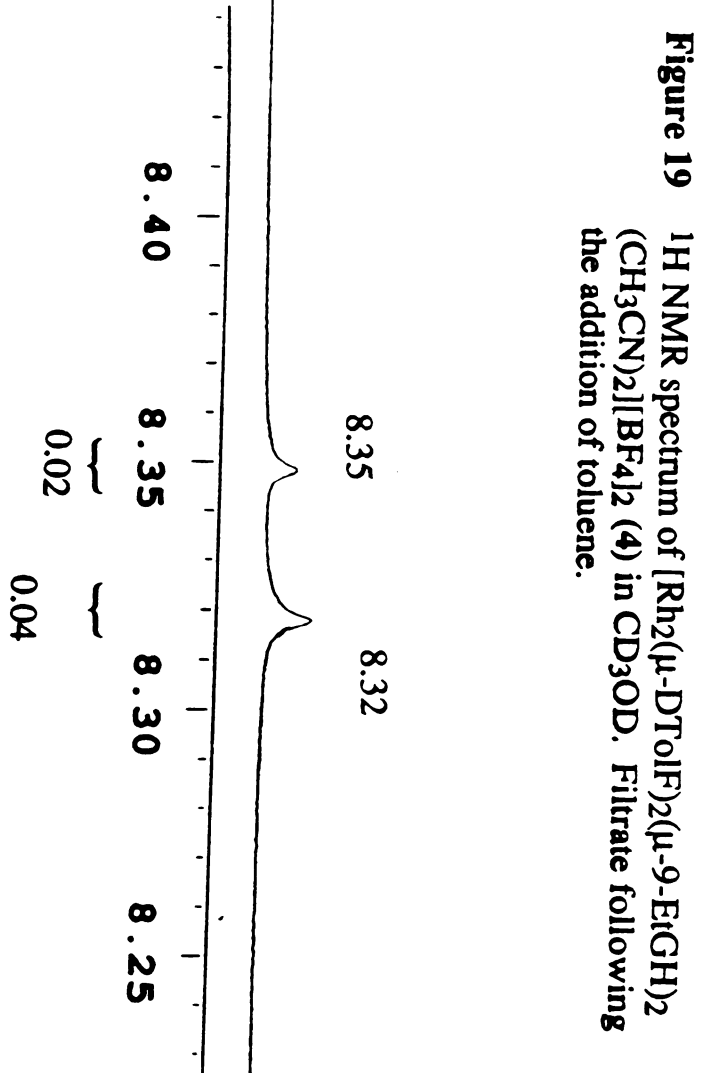




Table 5. Summary of crystallographic data for  $[Rh_2(\mu\text{-DTolF})_2(\mu\text{-9-EtGH})_2(CH_3CN)_2][BF_4]_2 \ (4)$ 

formula	Rh <sub>2</sub> C <sub>58</sub> H <sub>54</sub> N <sub>16</sub> B <sub>2</sub> F <sub>8</sub>
formula weight	1368.59
a, Å	21.98 (3)
b, Å	10.98 (1)
c, Å	23.21 (2)
α, deg	90
β, deg	105.32 (9)
γ, deg	90
V, Å3	5402 (10)
Z	4
temp, °C	-85 ± 2

nuclei such as <sup>1</sup>H, the paramagnetic term takes on a dominant role for the variation of the chemical shifts for heavier nuclei such as 103Rh. Blomberg et al. has published a simplified version of Ramsey's equation (Equation 2), the first term of which is the diamagnetic contribution.<sup>25b</sup> The second term consists of the following factors:  $\Delta E_{d-d}$ , the lowest d-d excitation energy; <r<sub>nd</sub>-3>, the d-orbital radii; D<sub>i</sub>, the imbalance of the dorbital electron population; and B, a constant. Hence the paramagnetic shielding term is dependent upon d-d electron transition energies ( $\Delta E$ ). A direct correlation between ligand field of the d<sup>7</sup>-d<sup>7</sup> Rh<sub>2</sub>IIL<sub>4</sub> complexes and the <sup>103</sup>Rh chemical shifts can be expected. Previous studies have revealed that, although certain ranges of chemical shifts for the different oxidation states can be discerned, the overlap of these shifts (Figure 18) prevents the absolute assignment of oxidation state based on <sup>103</sup>Rh chemical shifts. The reliable trend in <sup>103</sup>Rh NMR spectroscopy is the influence of the ligand field on the <sup>103</sup>Rh chemical shift within a series of related compounds. A higher  $\Delta E$  created by a strong ligand field should induce an upfield chemical shift. Conversely, a lower  $\Delta E$  should generate a downfield chemical shift.<sup>25a</sup> A review article by Mann further elaborates that when the paramagnetic term is small, the ligand field contribution would have only a minimal effect on  $\Delta E$ ; a small change in the ligand field would then be expected to have a large effect on the chemical shift when the paramagnetic term is large. This is in support of the findings reported by Blomberg, et al.25

# **Equation 2**

 $\delta = -A\rho_{\rm electrons} + (B\langle r_{\rm nd}^{-3}\rangle D_{\rm i}) \, / \, (\Delta E_{\rm d-d})$ 

It is of importance to note that <sup>103</sup>Rh NMR spectroscopy is highly temperature dependent. Large shifts in the <sup>103</sup>Rh NMR spectra of many compounds occur with temperature changes (~2 ppm/K). Thus, the precise temperature of the experiment must be known in order to accurately report the <sup>103</sup>Rh chemical shift within 1 ppm.

In addition, the dependence of the geometry of Rh compounds has also been observed to have dramatic effects on the chemical shift. A change from *cis* to *trans* geometry has been correlated with a downfield shift in all documented cases. Similarly, downfield shifts are observed when going from a *fac*- to a *mer* geometry.<sup>25a</sup>

Figure 20 -1573 - -1931 Rh(V)9931 - 1839 Rh (III) 7644 - 1395 Rh (II) 2344 - 1224 Rh (I) -1360 Rh (metal) 10000 8000 6000 4000 2000 -2000 ppm 0 <sup>103</sup>Rh chemical shift ranges.

# 2. 103Rh NMR Spectral Studies of Dirhodium Antitumor Agents

The  $^{103}$ Rh signal observed for (2) at  $\delta = 5551.98$  ppm represents a noticeable upfield shift from the signal observed for  $Rh_2(\mu-DTolF)_2(\mu-O_2CCF_3)_2(H_2O)_2$  at  $\delta = 5886.60$  ppm. This suggests that the ligand field strength of  $\mu$ -9-EtGH is somewhat stronger than that of  $\mu$ -trifluoroacetate. The shift observed for (2) can also be compared to the  $^{103}$ Rh NMR shift

found for the comparable compound  $Rh_2(mhp)_4$ , which is a singlet at  $\delta = 5745$  ppm.<sup>26</sup> Although the singlet observed for (2) is a good indication of a single of <sup>103</sup>Rh environment, recall that the <sup>1</sup>H NMR spectrum for this compound suggests the presence of two isomers. The <sup>103</sup>Rh NMR spectrum expected for the "head-to-tail" isomer should resemble the spectrum of  $Rh_2(mhp)_4$ , in which each Rh atom is equivalent. On the other hand, the <sup>103</sup>Rh NMR spectrum expected for the "head-to-head" isomer should contain a two doublet signal for the two magnetically inequivalent <sup>103</sup>Rh nuclei, akin to the <sup>103</sup>Rh NMR spectrum of the "dimer of dimers  $[Rh_2(mhp)_4]_2$ ". Note that the signal-to-noise ratio in the <sup>103</sup>Rh NMR spectrum of (2) is very poor, such that only a singlet for the presumably "head-to-tail" isomer is observed (Figure 19). The noisy baseline that is observed in the spectrum is attributed to severe problems in tuning the probe

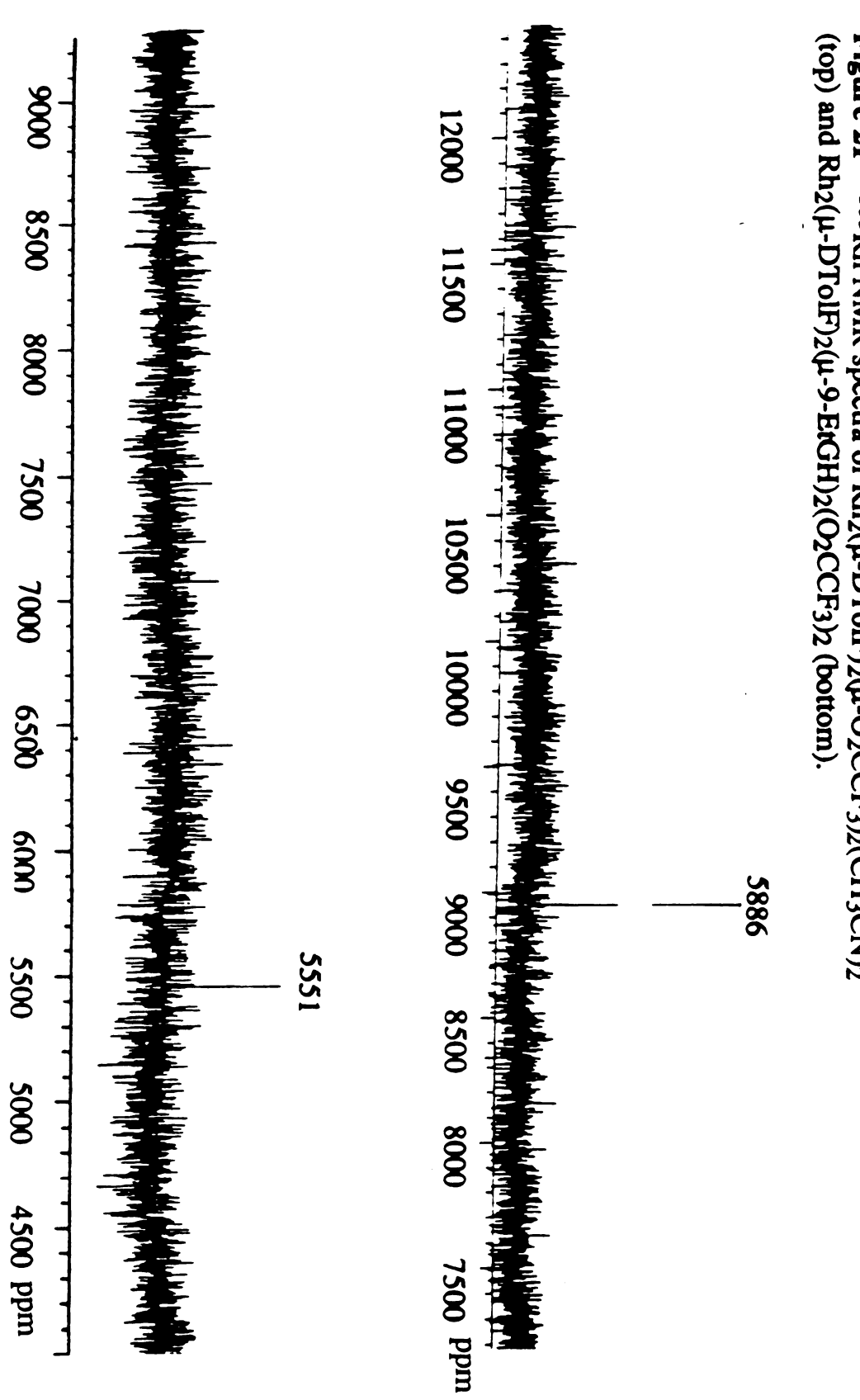
The  $^{103}$ Rh NMR spectrum of the partially solvated complex, (3), exhibits a singlet for the equivalent  $^{103}$ Rh nuclei at  $\delta = 4648.73$  ppm. The signal is observed  $\sim 1200$  ppm upfield from the signal observed for  $Rh_2(\mu-DPhF)_2(\mu-O_2CCF_3)_2(H_2O)_2$  in CD<sub>3</sub>CN. This indicates an increase of electron density on the dimetal core increasing the ligand field ( $\Delta E$ ), thereby increasing the shielding, and suggesting that the acetonitrile ligands are somewhat stronger donors than the trifluoroacetate ligands. The  $^{103}$ Rh spectrum observed for (3) is in accord with the results of the X-ray diffraction studies.

#### 4. Conclusion

Recent developments in our laboratories in the chemistry of dirhodium tetra-carboxylate compounds with DNA purines opens the question of the possible involvement of the O6 position in the observed

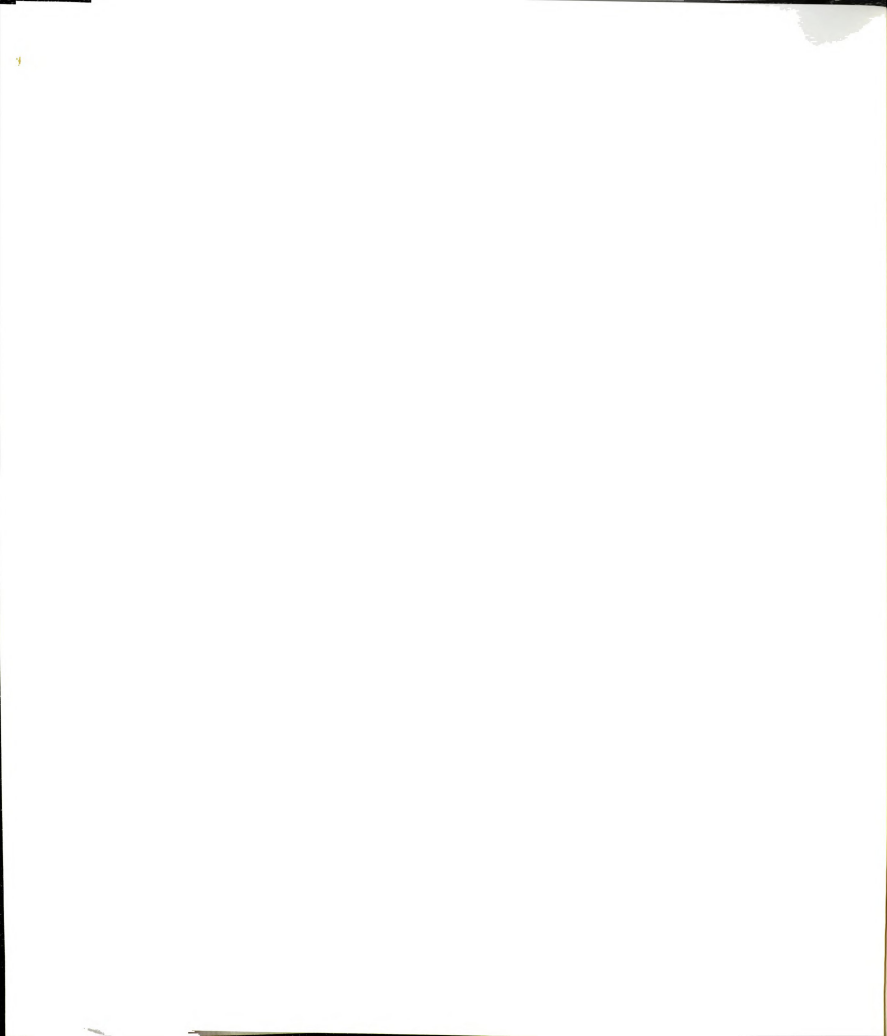
anticancer activity of this class of compounds. With the ultimate goal of increasing the antitumor activity displayed by dirhodium complexes, investigations of purine reactions of  $Rh_2(\mu\text{-form})_2(\mu\text{-O}_2CCF_3)_2(H_2O)_2$  and  $[Rh_2(\mu\text{-DTolF})_2(CH_3CN)_6]^{2+}$  have been explored. The products with 9-EtGH formed from the reactions with  $Rh_2(\mu\text{-form})_2(\mu\text{-O}_2CCF_3)_2(H_2O)_2$  and  $[Rh_2(\mu\text{-DTolF})_2(CH_3CN)_6]^{2+}$  show little or no preference for the formation of the "head-to-head" isomer over the "head-to-tail" isomer. These compounds, then, appear to react similarly to the dirhodium tetracarboxylate compounds that were previously studied in our laboratories, and will most likely exhibit similar and possibly more effective behavior *in vivo*. From this information, it is hoped that the possible binding modes responsible for the antitumor activity of the dirhodium complexes may be elucidated and compared to the growing database of chemistry for dinuclear anticancer agents.

Figure 21  $^{103}$ Rh NMR spectra of Rh<sub>2</sub>( $\mu$ -DTolF)<sub>2</sub>( $\mu$ -O<sub>2</sub>CCF<sub>3</sub>)<sub>2</sub>(CH<sub>3</sub>CN)<sub>2</sub> (top) and Rh<sub>2</sub>( $\mu$ -DTolF)<sub>2</sub>( $\mu$ -9-EtGH)<sub>2</sub>(O<sub>2</sub>CCF<sub>3</sub>)<sub>2</sub> (bottom).



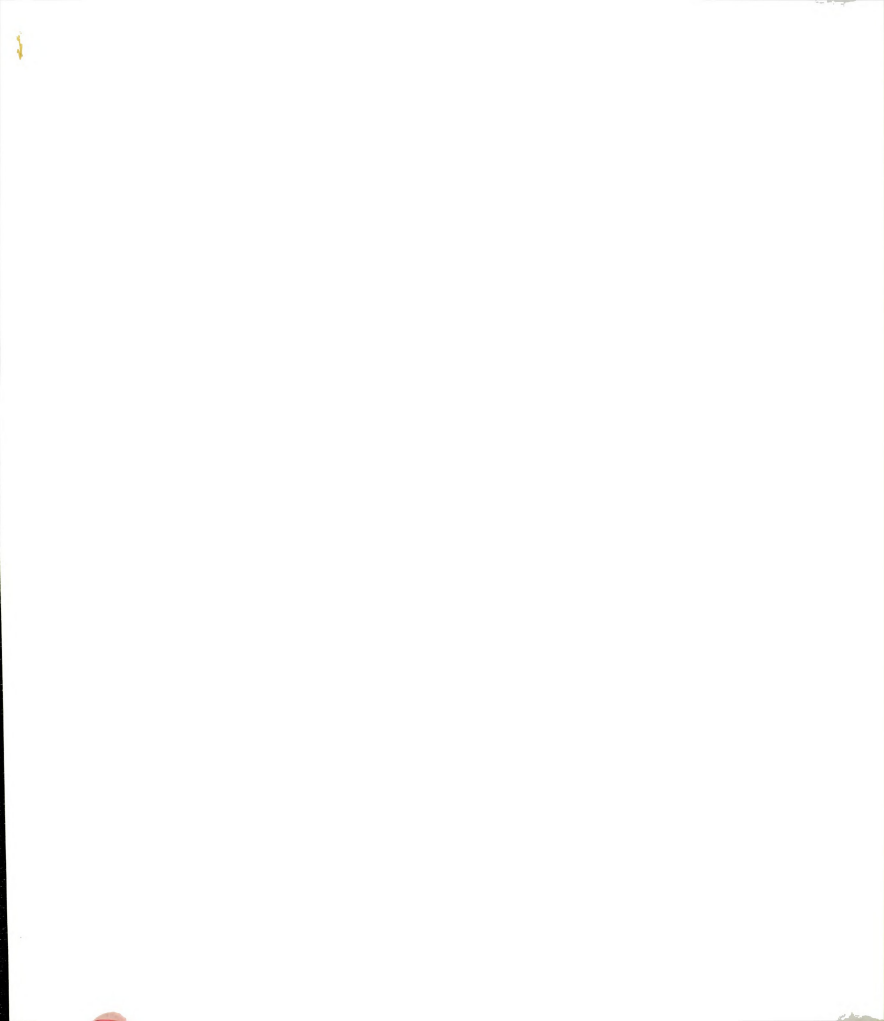
mdd

Figure 22  $^{103}$ Rh NMR spectrum of [Rh<sub>2</sub>( $\mu$ -DTolF)<sub>2</sub>(CH<sub>3</sub>CN)<sub>6</sub> ][BF<sub>4</sub>]<sub>2</sub> (3).



# Chapter III

**Dirhenium Anticancer Agents** 



#### 1. Introduction

Our discoveries of unique bridging modes for guanine and adenine bound to dinuclear transition metal compounds of rhodium and ruthenium directed our interest to yet another class of dinuclear transition metal complexes possessing the same lantern structure, namely Re<sub>2</sub>(III) bis- and tetra-carboxylates. The *cis*-bis- and tetra-carboxylates of dirhenium(III) have been known to exhibit carcinostatic activity, with results of *in vivo* tests supporting the inhibition of DNA synthesis as the primary target for antitumor activity. Previous antitumor studies of Re<sub>2</sub>( $\mu$ -O<sub>2</sub>CCH<sub>3</sub>)<sub>4</sub>(SO<sub>4</sub>) and *cis*-Re<sub>2</sub>( $\mu$ -O<sub>2</sub>CCR)<sub>2</sub>Br<sub>4</sub> (R = CH<sub>3</sub>, CH<sub>2</sub>CH<sub>3</sub>, CH<sub>2</sub>CH<sub>2</sub>CH<sub>3</sub>) (Figure 20) revealed inhibition of DNA akin to analogous dirhodium complexes, but decomposition of the compounds led to the administering of doses far too high for efficient antitumor activity. Interestingly, the researchers observed what appeared to be rhenium oxide decomposition deposits during the necropsies of their test animals.<sup>17</sup>

This research was initiated with the hypothesis that the N7, O6 bridging mode adopted by 9-EtGH in the dirhodium chemistry would also be observed in the dirhenium systems. The requirement of the dinuclear complex to easily undergo equatorial ligand exchange is the foundation on which the likelihood of observing a bridging mode for the purines is based. Although it has been previously stated that the bis- and tetra-carboxylates of dirhenium(III) were observed to slowly undergo decomposition with destruction of the dinuclear core, the complexes were nonetheless found to inhibit DNA *in vivo*.<sup>17</sup> Attempts in our laboratories to understand the nature of DNA interactions has focused on reactions with guanine derivatives such as 9-EtGH with dirhodium and diruthenium compounds. Once an understanding of the coordination chemistry that may be involved

in DNA inhibition is obtained, modification of the complexes to improve their ability to withstand the destruction of the quadruple bond will be investigated. Such tailoring is expected to improve the antitumor properties of the dirhenium compounds.

Figure 23

$$R = alkyl, S = solvent$$

### 2. Experimental

### A. Synthesis

All reactions were carried out under an argon atmosphere by using proper Schlenk-line techniques. The starting compounds, ( $^nBu_4N$ )<sub>2</sub>(Re<sub>2</sub>Cl<sub>8</sub>), ( $^nBu_4N$ )<sub>2</sub>(Re<sub>2</sub>Br<sub>8</sub>), cis-Re<sub>2</sub>( $\mu$ -O<sub>2</sub>CR)<sub>2</sub>Br<sub>4</sub>L<sub>2</sub>, trans-Re<sub>2</sub>( $\mu$ -O<sub>2</sub>CR)<sub>2</sub>Br<sub>4</sub>, Re<sub>2</sub>( $\mu$ -O<sub>2</sub>CR)<sub>4</sub>Cl<sub>2</sub>, and Re<sub>2</sub>( $\mu$ -O<sub>2</sub>CEt)<sub>4</sub>(SO<sub>4</sub>)·nH<sub>2</sub>O were prepared by literature methods.<sup>30</sup>

#### Preparation of cis-Re<sub>2</sub>(µ-9-EtG)<sub>2</sub>Br<sub>4</sub> (6)

An amount of cis-Re<sub>2</sub>( $\mu$ -O<sub>2</sub>CCH<sub>2</sub>CH<sub>3</sub>)<sub>2</sub>Br<sub>4</sub>(CH<sub>3</sub>OH)<sub>2</sub> (60 mg, 6.65 x 10<sup>-5</sup> mol) was dissolved in methanol (10 mL) and 9-EtGH (25 mg, 1.39 x 10<sup>-4</sup> mol) was added to the stirring solution. The mixture was refluxed for 24 h during which time the color changed from green to dark purple-brown. The solution was concentrated under reduced pressure and diethyl ether (7 mL) was added to afford a dark purple-brown precipitate. The reaction mixture was filtered in air, the purple-brown solid was washed with 3 x 15 mL of hexanes followed by 2 x 10 mL of diethyl ether, and dried *in vacuo*. The solid was reprecipitated from a methanol (10 mL) and diethyl ether (5 mL) mixture cooled at -10°C. The product was collected by filtration in air and washed with 2 x 5 mL of diethyl ether, and dried *in vacuo* (35 mg, 39 % yield). <sup>1</sup>H NMR (CD<sub>3</sub>OD)  $\delta$  ppm: 8.94 (s, H8), 4.17 (q, CH<sub>2</sub>), 1.44 (t, CH<sub>3</sub>). Electronic absorption spectrum (CH<sub>3</sub>OH)  $\lambda_{max}$ , nm ( $\epsilon$ ): 511 (3021), 326 (26,660), 318 (26,190).

Compound (6) was also prepared from the bis-carboxylate compounds cis-Re<sub>2</sub>( $\mu$ -O<sub>2</sub>CCH<sub>3</sub>)<sub>2</sub>Br<sub>4</sub>(CH<sub>3</sub>OH)<sub>2</sub> and cis-Re<sub>2</sub>( $\mu$ -O<sub>2</sub>CCH<sub>2</sub>CH<sub>2</sub>CH<sub>3</sub>)<sub>2</sub>Br<sub>4</sub>(CH<sub>3</sub>OH)<sub>2</sub> in nearly quantitative yields. Reactions involving the trans isomers also yield (6) in quantitative yields from the same synthetic approach.

# Preparation of $Re_2(\mu-9-EtG)_2(\mu-O_2CCH_3)_4Cl_2$ (7)

Two equivalents of 9-EtGH (23 mg,  $1.28 \times 10^{-3}$  mol) were added to a suspension of  $Re_2(\mu\text{-}O_2CCH_3)_4Cl_2$  (52 mg,  $6.40 \times 10^{-5}$  mol) and  $CH_3CN$  (15 mL) and  $CH_3OH$  (2 mL) and the mixture was stirred at room temperature for 24 h. A red-brown solid precipitated which was collected by filtration in air. The compound was redissolved in  $CH_3CN$  and precipitated by addition of  $Et_2O$  and hexanes. The resulting precipitate

was washed with 2 x 5 mL of diethyl ether and dried *in vacuo* (23 mg, 34 % yield). <sup>1</sup>H NMR (CD<sub>3</sub>OD) δ ppm: 8.43(s, H8), 4.12 (q, CH<sub>2</sub>), 1.48 (m, CH<sub>3</sub>).

### Preparation of Re<sub>2</sub>( $\mu$ -9-EtG)<sub>2</sub>( $\mu$ -O<sub>2</sub>CCH<sub>2</sub>CH<sub>3</sub>)<sub>2</sub>Cl<sub>2</sub> (8)

- (a) A mixture of Re<sub>2</sub>(μ-O<sub>2</sub>CCH<sub>2</sub>CH<sub>3</sub>)<sub>4</sub>Cl<sub>2</sub> (103 mg, 1.18 x 10<sup>-4</sup> mol) and CH<sub>3</sub>CN (10 mL) was treated with two equivalents of 9-EtGH (56 mg, 3.13 x 10<sup>-4</sup> mol). Upon addition of methanol (~2 mL) the reaction color immediately changed from salmon to orange. The mixture was allowed to stir for an additional 2.5 h during which time a finely divided red-brown precipitate was observed to form. The solid was filtered in air and dried *in vacuo* (10 mg 7.8 % yield). <sup>1</sup>H NMR (CD<sub>3</sub>OD) δ ppm: 8.45 (s, H8), 4.11 (q, CH<sub>2</sub>), 3.81 (q, CH<sub>2</sub>), 1.48 (m, CH<sub>3</sub>).
- (b) A solution of Re<sub>2</sub>(μ-O<sub>2</sub>CCH<sub>2</sub>CH<sub>3</sub>)<sub>4</sub>Cl<sub>2</sub> (52 mg, 7.07 x 10<sup>-5</sup> mol) and CH<sub>3</sub>CN (15 mL) was combined with two equivalents of AgBF<sub>4</sub> (30 mg, 1.54 x 10<sup>-4</sup> mol) and the salmon colored mixture was allowed to stir for 12-18 h. During this time the mixture became yellow-brown in color. The reaction mixture was filtered through a Celite plug, two equivalents of 9-EtGH (27 mg, 1.51 x 10<sup>-4</sup> mol) were added to the filtrate, and the mixture was stirred for 2 h, after which time CH<sub>2</sub>Cl<sub>2</sub> (5 mL) was added to afford the precipitation of excess Ag salts. The mixture was filtered in air and the filtrate was concentrated under reduced pressure to yield a brown residue (22 mg, 32 % yield). <sup>1</sup>H NMR (CD<sub>3</sub>OD) δ ppm: 8.80 (s, H8), 4.16 (q, CH<sub>2</sub>), 3.8, (m, CH<sub>2</sub>), 1.44 (t, CH<sub>3</sub>), 1.27 (t, CH<sub>3</sub>).
- (c) A solution of  $Re_2(\mu-O_2CCH_2CH_3)_4(SO_4)\cdot nH_2O$  (30 mg, 3.56 x  $10^{-5}$  mol) and CH<sub>3</sub>CN (15 mL) was combined with two equivalents of 9-EtGH (12.7 mg, 7.12 x  $10^{-5}$  mol) and the mixture was stirred for 24 h. The mixture, which turned red-brown during this time, was filtered in air

and concentrated under pressure to yield a red-brown solid (19 mg, 59 % yield).  $^{1}$ H NMR (CD<sub>3</sub>OD)  $\delta$  ppm: 8.02 (s, H8), 4.15 (q, CH<sub>2</sub>), 4.09 (q, CH<sub>2</sub>), 1.35 (t, CH<sub>3</sub>), 1.28 (t, CH<sub>3</sub>).

### Preparation of Re<sub>2</sub>( $\mu$ -9-EtG)<sub>2</sub>( $\mu$ -O<sub>2</sub>CC<sub>6</sub>H<sub>6</sub>)<sub>2</sub>(CH<sub>3</sub>CN)<sub>2</sub>(BF<sub>4</sub>)<sub>2</sub> (9)

The tetra-benzoate complex (63 mg, 6.79 x 10<sup>-5</sup> mol) was suspended in CH<sub>3</sub>CN (25 mL), treated with AgBF<sub>4</sub> (26 mg, 1.34 x 10<sup>-4</sup> mol) and stirred for 24 h. The green-brown mixture was filtered through a Celite plug and reacted with two equivalents of 9-EtGH (20 mg, 1.11 x 10<sup>-4</sup> mol) for 12-16 h. The brown mixture was filtered in air, and the filtrate was concentrated under reduced pressure to afford a brown residue. The solid was dissolved in CH<sub>3</sub>CN (8 mL), precipitated with toluene (15 mL) and collected by filtration. The solid was washed with 2 x 10 mL of toluene and hexanes (35 mg, 45 % yield). <sup>1</sup>H NMR (CD<sub>3</sub>OD) δ ppm: 8.02 (s, H8), 7.43-8.00 (m, phenyl), 4.24 (m, CH<sub>2</sub>), 1.94 (s, *ax*-CH<sub>3</sub>CN), 1.50 (t, CH<sub>3</sub>).

## B. X-ray Crystallography

The structure of cis-Re<sub>2</sub>( $\mu$ -O<sub>2</sub>CH<sub>2</sub>CH<sub>3</sub>)<sub>2</sub>Br<sub>4</sub>(DMF)<sub>2</sub> (10) (DMF = dimethylformamide) was determined using general applications that have been described elsewhere. Geometric and intensity data were collected on a Rigaku AFC6S diffractometer with graphite-monochromated MoK<sub> $\alpha$ </sub> ( $\lambda_{\alpha}$  = 0.71069 Å) radiation and were corrected for Lorentz and polarization effects. The calculations used for the structure determination were performed with VAX computers on a cluster network within the Department of Chemistry at Michigan State University using the Texsan software package of the Molecular Structure Corporation.<sup>23,24</sup> cis-Re<sub>2</sub>( $\mu$ -O<sub>2</sub>CH<sub>2</sub>CH<sub>3</sub>)<sub>2</sub>Br<sub>4</sub>(DMF)<sub>2</sub> (10)

(I) Data Collection and Reduction. Large single crystals of (10) were obtained from a DMF solution of cis-(Re<sub>2</sub>( $\mu$ -

 $O_2CH_2CH_3)_2Br_4(CH_3OH)_2$  that had been cooled to ~-10 °C for 2-3 days. A suitable single crystal with the approximate dimensions of 0.518 x 0.181 x 0.415 mm<sup>3</sup> was mounted on the tip of a glass fiber with Dow Corning grease. Cell constants were obtained from a least squares refinement using 24 carefully centered reflections in the range 29° < 2θ < 37°. Data were collected at -100 ± 2 °C by using the ω-scan method in the range 4 ≤ 2θ ≤ 47°. Weak reflections (those with F < 10σ(F)) were rescanned at a maximum of 2 rescans and the counts were accumulated to ensure good counting statistics. A total of 3918 reflections were collected. Of the total data collected, 1922 reflections were unique data with  $F_0^2 > 3σ(F_0)^2$ . Periodic measurement of three representative reflections at regular intervals revealed that a 13% loss of diffraction intensity had occurred during data collection. A decay correction was applied to account for the phenomenon. An empirical absorption correction was applied on the basis of azimuthal scans of 3 reflections with χ near 90°.

(ii) Structure Solution and Refinement. The positions of all non-hydrogen atoms were obtained by application of the direct methods. With the exception of two atoms, all atoms were refined with anisotropic thermal parameters. Hydrogen atoms were treated as fixed contributors at idealized positions and were not refined. Disorder in the structure caused certain atoms to refine as non-positive definite. The current least squares refinement of 235 parameters gave residuals of R = 0.077 and  $R_w = 0.093$  and a goodness-of-fit = 2.93. A final difference Fourier map revealed the highest peak in the difference map to be  $2.6 \text{ e}^{-}/\text{Å}^3$ .

#### 3. Results

#### A. Crystallographic Properties of (10)

The crystal structure of (10), the reported antitumor active dirhenium(III) bis-carboxylate, was determined to verify the cis arrangement of the propionate ligands.<sup>26,30</sup> Recall that one of the criteria for antitumor activity observed for cisplatin and its related compounds is the presence of cis labile groups. Crystal parameters and basic information pertaining to data collection are summarized in Table 6. The Pluto representation of (10) is depicted in Figure 21 and selected bond distances and angles are summarized in Table 7.

Compound (10) crystallizes in the monoclinic-P crystal system. Although a certain amount of disorder that involves the carboxylate ligands and the bromide ligands is evident, a cisoid arrangement of the propionate ligands was confirmed. The Re-Re bond distance (2.248 (2) Å) is consistent with other quadruply bonded compounds of this type (Re-Re bond distances ~2.25 Å). The compound conforms with the previously established pattern of the bis-carboxylates which will be discussed in the next section.<sup>7</sup>

### B. Spectroscopic Properties of (6)

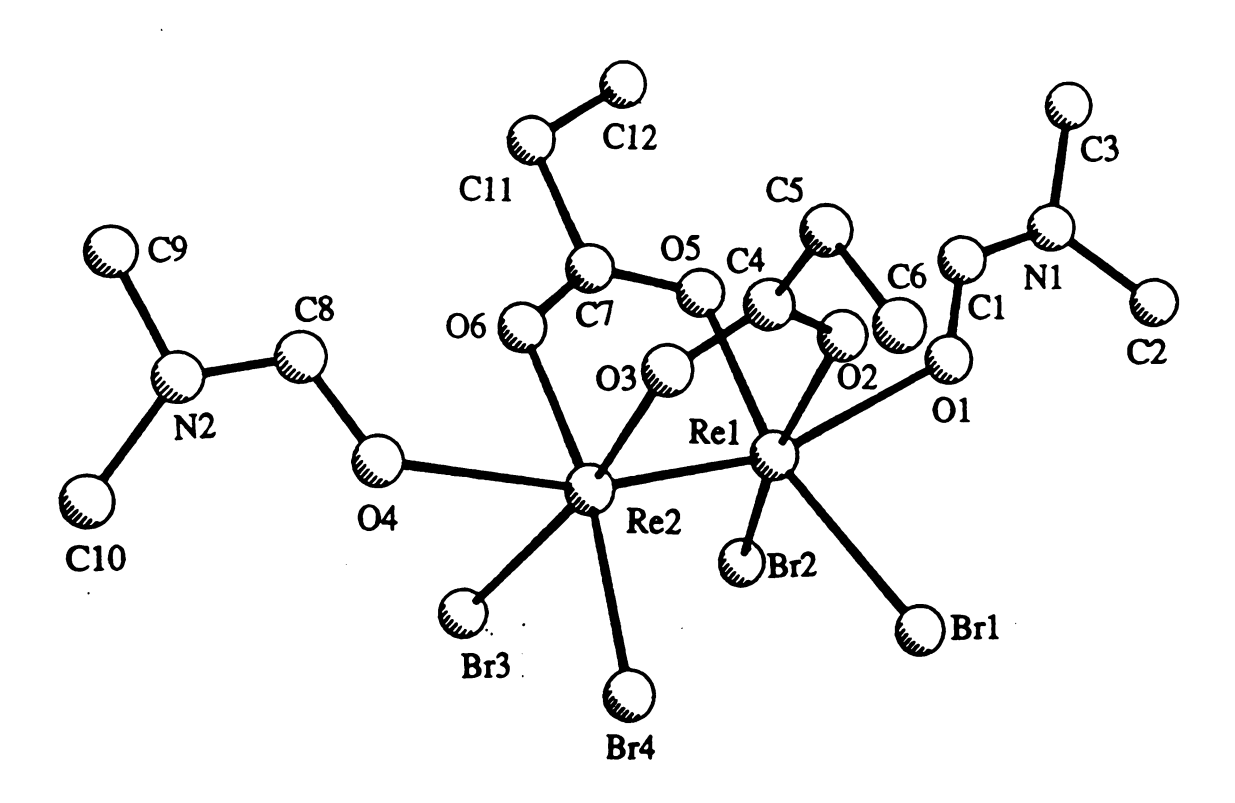
The structure of (6) was deduced from the <sup>1</sup>H NMR and UV-visible spectral studies and from extrapolation of the structural and chemical properties of the *cis*-bis-carboxylates.<sup>26,30</sup> Unlike the results found for the analogous the dirhodium chemistry, the <sup>1</sup>H NMR spectrum of (6) (Figure 22) in CD<sub>3</sub>OD exhibits only one singlet in the H8 region (8.94 ppm), which suggests that only one product is formed in the reaction. This is a dramatic shift of the H8 resonance compared to free 9-EtGH which is commonly observed at ~7.6 ppm in CD<sub>3</sub>OD. The quartet centered at 4.17 ppm is

Table 6. Summary of crystallographic data for Re<sub>2</sub>(μ-O<sub>2</sub>CCH<sub>2</sub>CH<sub>3</sub>)<sub>2</sub>Br<sub>4</sub>(DMF)<sub>4</sub> (10)

formula	Re <sub>2</sub> C <sub>12</sub> H <sub>24</sub> N <sub>2</sub> Br <sub>4</sub> O <sub>6</sub>
formula weight	984.36
space group	P2 <sub>1/n</sub>
a, Å	9.825 (7)
b, Å	13.258 (3)
c, Å	18.433 (4)
α, deg	90
β, deg	93.13 (9)
γ, deg	90(0)
V, Å3	2397 (2)
Z	4
d <sub>calc</sub> , g/cm <sup>3</sup>	2.727
μ (MoKα), cm <sup>-1</sup>	168.59
temp, °C	-100 ± 2
Ra	0.077
R <sub>w</sub> b	0.093

a R=  $\sum ||F_0| - |F_c||/\sum |F_0|$ . b R<sub>w</sub> =  $[\sum w(|F_0| - |F_c|)^2/\sum w|F_0|^2]^{1/2}$ ; w =  $1/\sigma^2(|F_0|)$ 

Figure 24



PLUTO Representation of Re<sub>2</sub>(O<sub>2</sub>CCH<sub>2</sub>CH<sub>3</sub>)<sub>2</sub>Br<sub>4</sub>(DMF)<sub>2</sub>

Table 7. Selected bond distances and bond angles for  $Re_2(\mu\text{-}O_2CCH_2CH_3)_2Br_4(DMF)_2$  (10)

# **Bond Distances**

A	В	A-B (Å)	A	В	<b>A-B</b> (Å)
Re1	Re2	2.248(2)	Re1	O1	2.34(3)
Re1	O2	2.02(3)	Re1	O5	2.04(3)
Re2	O3	2.07(3)	Re2	O6	1.99(3)
Re2	O4	2.47(3)	Re1	Br1	2.455(5)
Re1	Br2	2.452(5)	Re2	Br3	2.457(5)
Re2	Br4	2.467(4)			

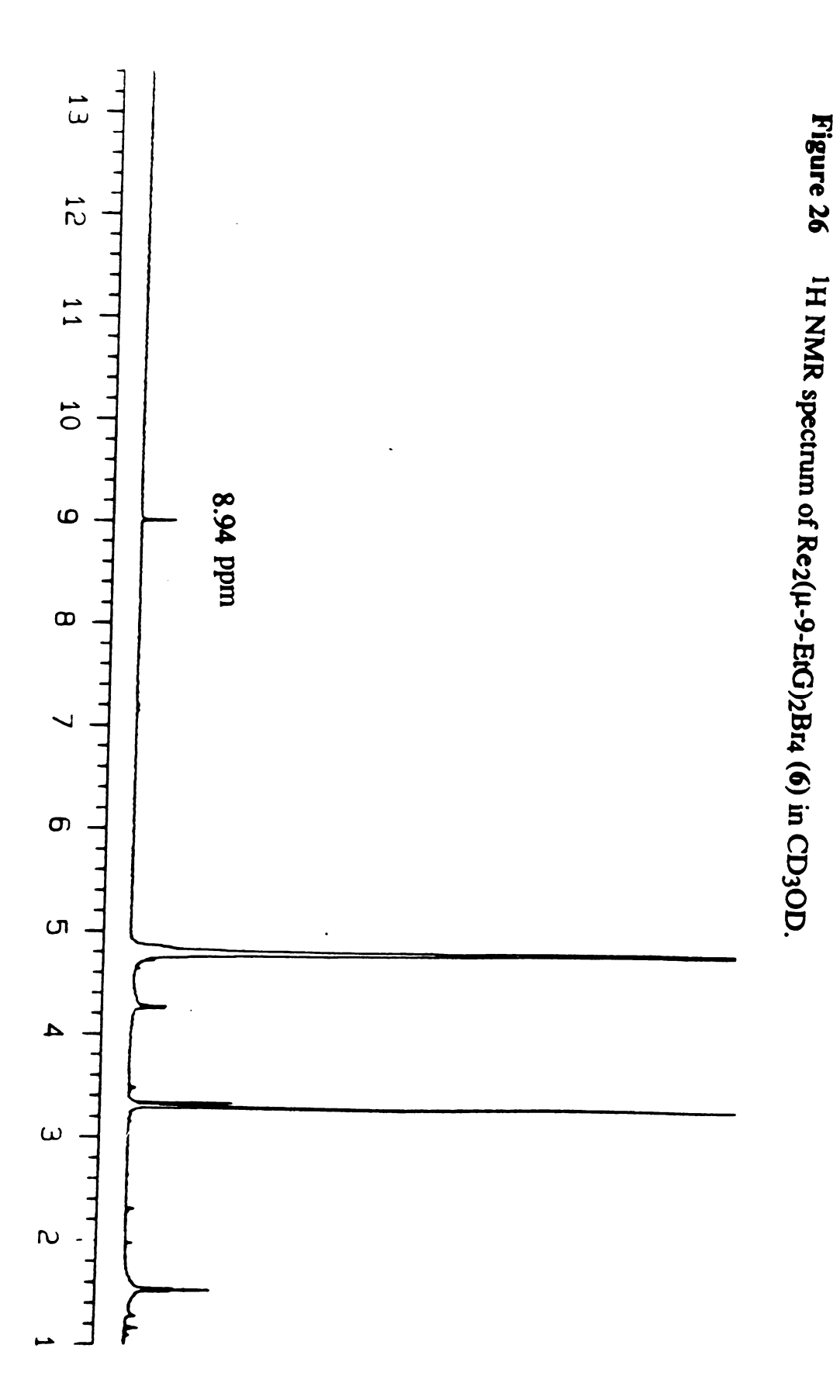
# **Bond Angles**

A	В	С	A-B-C (0)
Re1	Re2	Br1	105.1(1)
Re2	Re1	Br2	104.7(1)
Re1	Re2	Br3	104.3(1)
Re1	Re2	Br4	104.6(1)
O2	C4	O3	116(4)
O5	C7	O6	127(5)

attributed to the CH<sub>2</sub> protons of the 9-ethyl group. The triplet centered at 1.43 ppm is the resonance expected for the shifted methyl protons of the 9-ethyl group. No signals are observed for bound carboxylates, thus implying that a substitution of these ligands for the purines has occurred. Another feature discerned from the spectrum is that no signal for axial solvent molecules was observed.

The presence of one H8 signal does not provide sufficient information as to whether the 9-EtGH ligands are bound to the dirhenium center in the "head-to-head" or "head-to-tail" fashion since a center of symmetry exists in both proposed isomers relating the bound purines (Figure 23). The indication of one isomer being formed counters the trend observed in the chemistry of the dirhodium systems, for which both isomers were observed in reactions of the *cis*- and *tetra*-acetate compounds. It appears that the substitution of trifluoroacetate proceeds with specific formation of only one product whereas the acetate displacement leads to both possible isomers.

Figure 25



The most likely structure for compound (6) is a cis orientation of the purines, since the compounds of the type  $Re_2(\mu-L)_2X_4S_2$  (L = bridging ligand, X = halide, S = solvent) tend to adopt this configuration with the presence of at least two solvent molecules in the axial positions.<sup>26,30</sup> For example, except for a few rare cases, the cis-bis-carboxylates of dirhenium(III) all contain the carboxylate ligands in the cis positions as long as axial solvent molecules are present.<sup>26,31</sup> It has been proven that removal of the axial ligands occurs when heating the bis-carboxylate compounds above 250 °C. At these temperatures, the dirhenium(III) bis-carboxylates sublime and isomerize to the trans derivatives in the vapor phase (Figure 24). The trans-bis-carboxylates adopt a polymeric structure with the halides assuming pseudo axial-equatorial positions which bridge the dimetal centers. The cis-trans isomerization is reversible in solution upon addition of neutral donor solvents.<sup>26</sup>

Figure 27

R = alkyl

Unless axial solvent molecules are displaced in the NMR solvent, there is no spectroscopic evidence for the presence of axial solvent molecules bound to (6). Compound (6) is suspected to contain the deprotonated 9-EtG- ligand bridging the dimetal center in a cisoid fashion through the N6 and O7 positions similar to other dimetal systems with this purine. One possibility is that (6) is an extended structure with the equatorial Br- atoms of one dinuclear center bridging a second dinuclear center through its axial positions (Figure 25). It is unlikely that a cis-trans isomerization occurred in the reaction, since the temperature was maintained at the boiling point of methanol (~65 °C), and it has not been shown that cis-trans isomerization occurs except at extremely high temperatures and in the solid state. It cannot be ruled out, however, that the purine could be bound in a transoid configuration since a center of symmetry relating the bound purines would also exist, but only X-ray crystallography can confirm the arrangement of the ligands.

The purine ligand present in compound (6) is expected to be the anionic form of the ligand since the pK<sub>b</sub>'s of the carboxylates present (CH<sub>3</sub>CO<sub>2</sub>-, 9.25; CH<sub>3</sub>CH<sub>2</sub>CO<sub>2</sub>-, 9.13; CH<sub>3</sub>CH<sub>2</sub>CH<sub>2</sub>CO<sub>2</sub>-, 9.19) in the starting compounds are within the range of the well documented pK<sub>a</sub> of the N1 position of bound 9-EtGH which is lowered upon metal binding from ~9.4 to ~8.0.<sup>7</sup> The topic of the deprotonation of the N1 position was treated in the previous chapter.

X-ray crystallographic studies to verify the spectroscopic assignments of (6) are in order. A crystal structure would ascertain which isomer is the preferred isomer formed in the reaction and would confirm

Figure 28

"head-to-head"

"head-to-tail"

the possible extended structure previously described. Attempts to crystallize (6) are underway. The solubility of (6) is limited to H<sub>2</sub>O and CH<sub>3</sub>OH which leaves very few choices of solvent combinations. All of the combinations that were tried led to the conclusion that this compound tends to form an amorphous solid. Derivatization of (6) by substituting the coordinated Br<sup>-</sup> ligands for solvents groups in the presence of non-coordinating anions such as [PF6]<sup>-</sup> in hopes of obtaining a compound with better crystal packing properties were tried with little success.

#### C. Spectroscopic Properties of (7)

As is the case of (6), compound (7) is only slightly soluble in water and methanol. The <sup>1</sup>H NMR spectrum of (6) was contaminated by

unreacted starting materials and unknown impurities. Attempts to purify the product by reprecipitation resulted in major loss of the sample. No further attempts to repeat this reaction were made since the biological studies of  $Re_2(\mu-O_2CCH_3)_4Cl_2$  indicated that the propionate analog of this complex exhibited far greater antitumor activity.

#### D. Spectroscopic Properties of (8)

(a) One of the problems associated with investigating the properties of the *tetra*-acetate of dirhenium(III) is the relatively strong binding interactions of the axial chlorides, which result in low solubility and slow substitution reactions. The more biologically relevant *tetra*-carboxylate of dirhenium(III), the *tetra*-propionate derivative, is far more soluble than its acetate analog simply because of the presence of the more soluble propyl substituents. The presence of strongly bound axial halides in the dirhenium tetra-carboxylates, in general, require that substitution reactions take place not axially, but *via* dissociation of the equatorial ligands, thus causing reactions to be very sluggish. Equatorial attack of the Re2<sup>6+</sup> core is rationalized by the necessity for deprotonation and displacement of the propionate ligands to occur simultaneously (Figure 26).

Although the poor yield of this reaction is discouraging, the <sup>1</sup>H NMR spectrum of (8a) in CD<sub>3</sub>OD exhibits a broad singlet in the H8 region of 9-EtGH at 8.45 ppm which verifies that a reaction did indeed take place (Figure 27). The H8 region of this spectrum also shows a broad signal of multiplets centered at approximately 8.0 ppm. This suggests that several products are being formed in this reaction. Reprecipitation of the compound from CH<sub>3</sub>CN with Et<sub>2</sub>O and hexanes allowed for the separation of the major product from the impurities. The <sup>1</sup>H NMR spectrum in

CD<sub>3</sub>CN indicates that unreacted dirhenium *tetra*-propionate was also present.

(b) The [BF<sub>4</sub><sup>-</sup>] salt of Re<sub>2</sub>(μ-O<sub>2</sub>CCH<sub>2</sub>CH<sub>3</sub>)<sub>4</sub>Cl<sub>2</sub> is generated *in situ* by the addition of two equivalents of AgBF<sub>4</sub> in order to help facilitate the reaction with 9-EtGH. Without the presence of the axial chloride ligands, the Re<sub>2</sub><sup>6+</sup> unit has available the axial and equatorial sites for attack by the purine. The <sup>1</sup>H NMR spectrum of (8b) in deuterated methanol exhibits only one signal in the H8 region of 9-EtGH at 8.80 ppm. This chemical shift is analogous to the corresponding value observed in the spectrum of (6). The quartet observed at 4.15 ppm is attributed to the CH<sub>2</sub> protons of 9-ethyl substituent while the quartet at 4.09 ppm can be assigned to the CH<sub>2</sub> protons of the bound propionate ligands. The CH<sub>3</sub> protons resonate at 1.28 and 1.35 ppm for the bound propionate and 9-ethyl group on the guanine, respectively.

Analogous to the reactions of the tetra-carboxylates of dirhodium and diruthenium with 9-EtGH, cis substitution of two acetates is expected to occur for the compounds  $Re_2(\mu-O_2CR)_4X_2.^{26}$  The observed trend for these molecules to undergo cis substitution as the more energetically favored pathway has been established.<sup>26</sup> Thus the proposed structure of (8b) would be similar to the structure of  $Rh_2(\mu-9-EtG(H))_2(\mu-O_2CR)_2L_2$  wherein the purine ligands are arranged in a cis configuration with respect to each other.<sup>19</sup> Furthermore, the bound 9-EtGH is expected to be deprotonated at the N1 position due to the basicity of the propionate leaving groups (pK<sub>b</sub> ~9.13).

It was also hoped that the presence of different ligands such as the propionate ligands might aid in the isolation of single crystals suitable for X-ray crystallography. Recall that compound (6) is suspected to exhibit

poor crystal packing arrangements leading to amorphous solids. Unfortunately, similar properties were also observed for (8b).

(c) The [SO<sub>4</sub>]<sup>2-</sup> salt of the *tetra*-propionate complex was found to decompose in water, but is quite stable in CH<sub>3</sub>CN. The <sup>1</sup>H NMR spectrum of this compound shows that the reaction does not proceed cleanly, as evidenced by the <sup>1</sup>H NMR spectrum depicted in Figure 28. The resonance for the H8 region of 9-EtGH is assigned to the signal observed at 8.00 ppm. Both the quartet and triplet expected for the methylene and methyl protons of the purine are observed at 4.15 and 1.35 ppm, respectively. The methylene and methyl protons of bound propionate are found at 4.09 and 1.28 ppm, respectively. The spectrum also exhibits signals for unreacted starting material. The compound (8c) is proposed to exhibit a structure similar to (8b) as evidenced by <sup>1</sup>H NMR spectroscopy which supports the assignment of two bound 9-EtG- and two bound propionate ligands.

# E. Spectroscopic Properties of (9)

The difficulty in crystallizing the compounds (6)-(8) led us to investigate possible model compounds that might possess enhanced crystal packing properties. Unfortunately, compound (9) precipitates from solution to form amorphous solids. The pK<sub>b</sub> of the benzoate ligands (~9.81) is well within the range for deprotonation of the N1 position of 9-EtGH to occur, therefore it is expected that the deprotonated form of the purine is present. It would also seem to appear that the trend of only one isomer being formed in the dirhenium(III) chemistry is upheld. The <sup>1</sup>H NMR spectrum of (9) indicates only one H8 proton at 8.02 ppm, which is shifted downfield from the H8 signal from ~7.6 ppm for the free ligand. The aromatic protons of the benzoate ligands resonate in the range of 7.43-8.00 ppm. The CH<sub>2</sub> protons of the purines are observed in the expected

region at 4.24 ppm in a 1:1 ratio with the benzoate protons. The triplet antipicipated for the CH<sub>3</sub> protons of 9-EtG<sup>-</sup> are assigned to the signal at 1.50 ppm. As determined from the integration, two of the benzoate groups are bound to the metal in a 1:1 ratio with 9-EtG<sup>-</sup>. By analogy to the compounds formed from dirhenium(III) tetra-carboxylates and 9-EtGH, (9) is expected to contain a *cis* configuration of its equatorial ligands. The presence of the <sup>1</sup>H NMR signal at 1.94 ppm suggests that acetonitrile groups occupy the axial positions of the dinuclear unit and are exchanged in the NMR solvent.<sup>2</sup>

#### 4. Conclusion

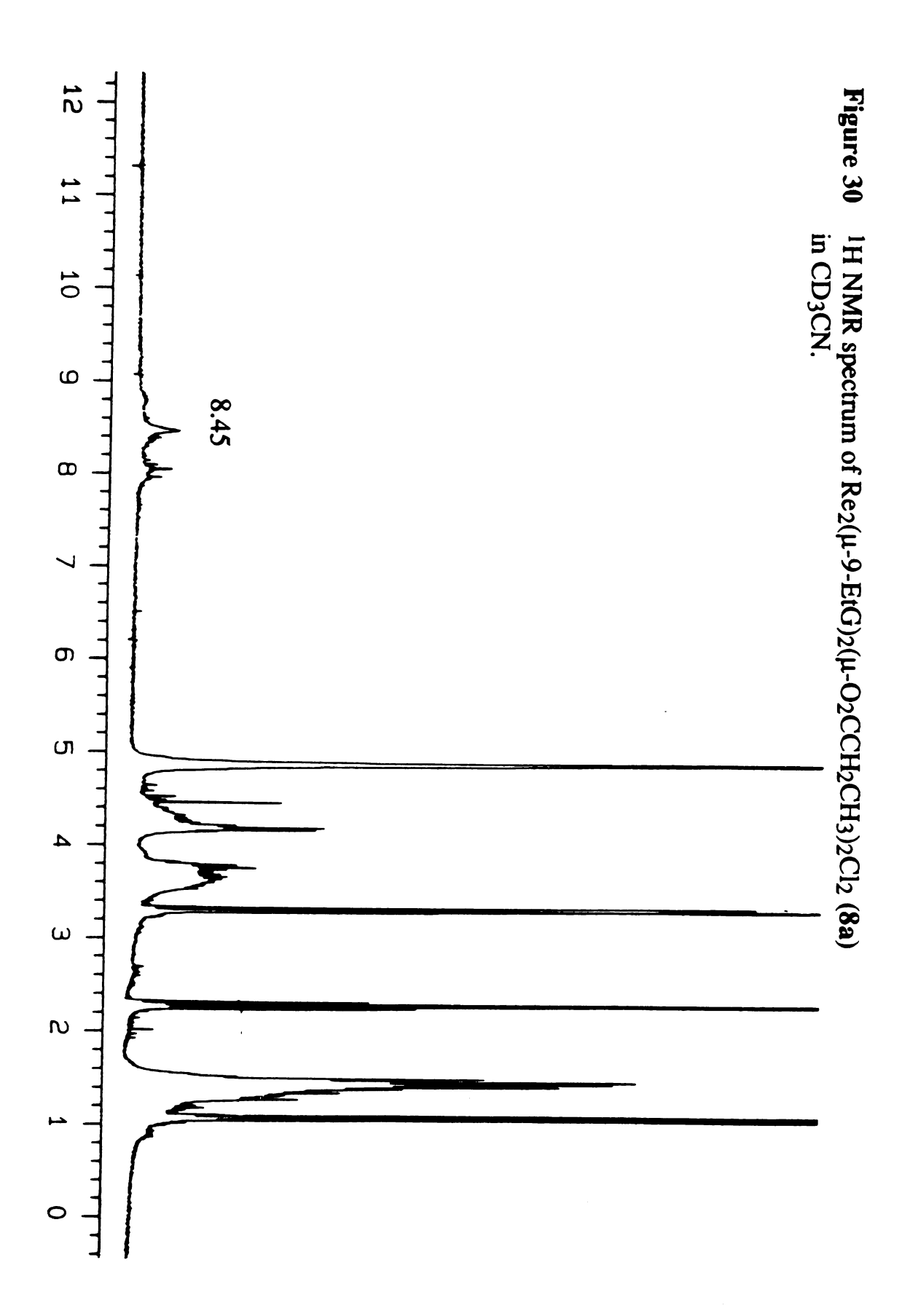
The investigation of dirhenium compounds as antitumor agents has been largely ignored by the medical community due to the large amounts of compound required to effectively inhibit tumor growth. It has been noted that the reason for high dosage rates of dirhenium tetra-carboxylates is that compounds of this type readily decompose *in vivo*.<sup>3</sup> No prior investigations of the coordination chemistry of these systems with DNA nucleic acids has been investigated. Furthermore, no attempts to tailor the ligand environment to prevent facile decomposition under physiological conditions have been reported.

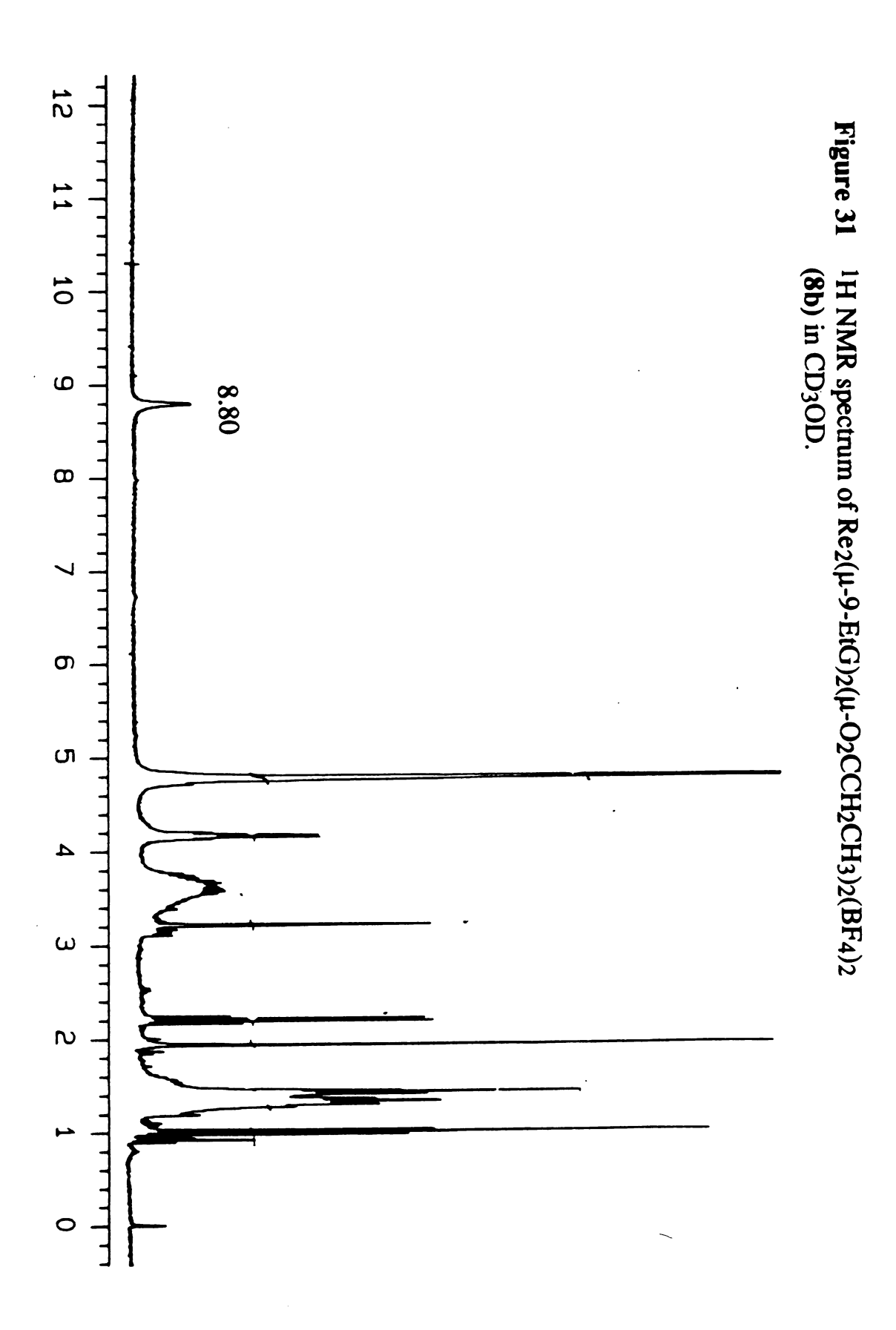
It has been found that compounds of dinuclear rhenium(III) bind to the model DNA nucleobase 9-ethylguanine. The reactions proceed via substitution of two cis carboxylate ligands for two deprotonated 9-ethylguanine ligands. It has been observed that the products form only one of the two possible isomers. The establishment of this product as the "head-to-head" or "head-to-tail" isomer must be provided by X-ray crystallography. Regardless of the isomer question, it is expected that the

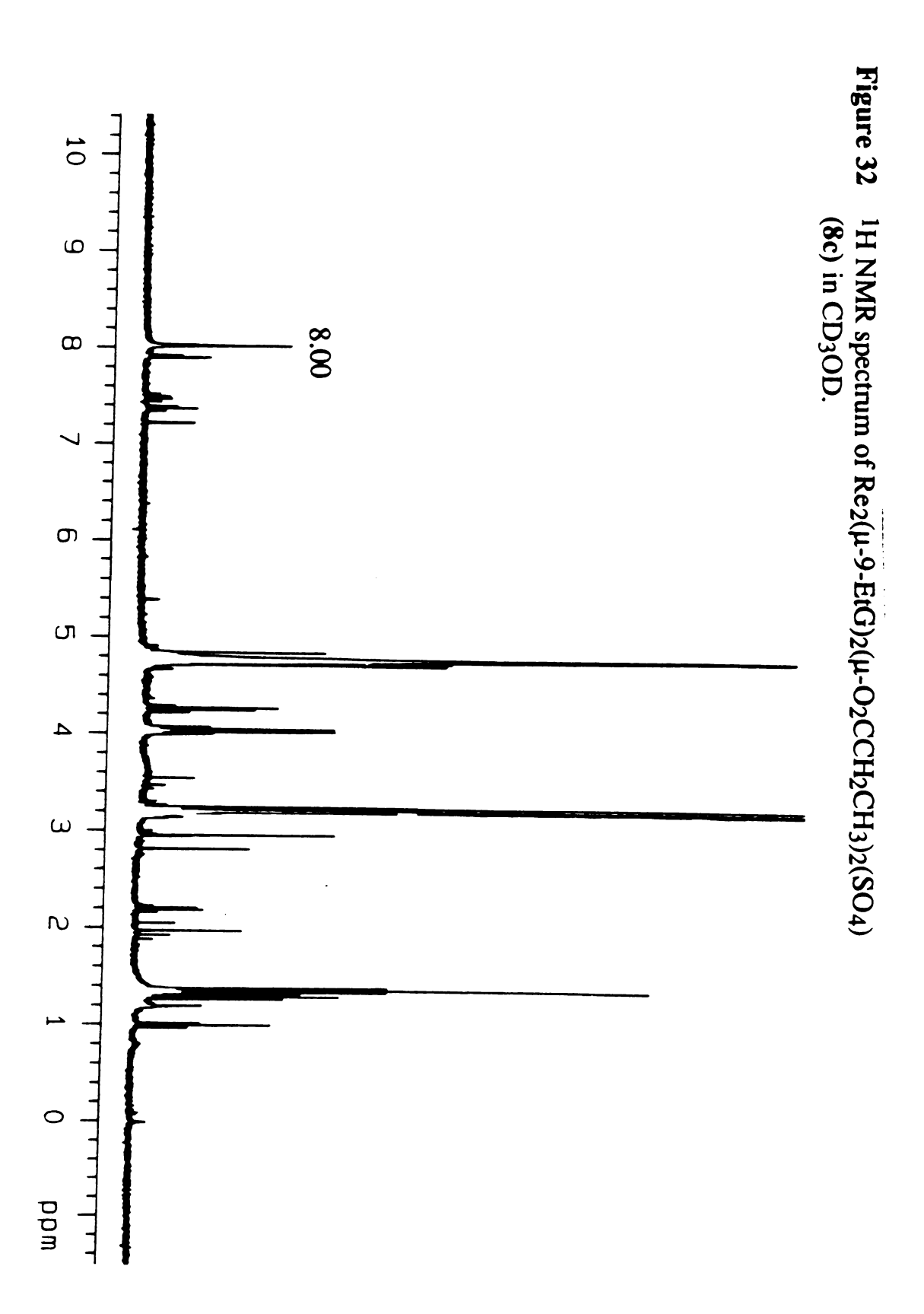
X-ray study will confirm that two purines bridge the dinuclear center through the O6 and N7 positions in all cases.

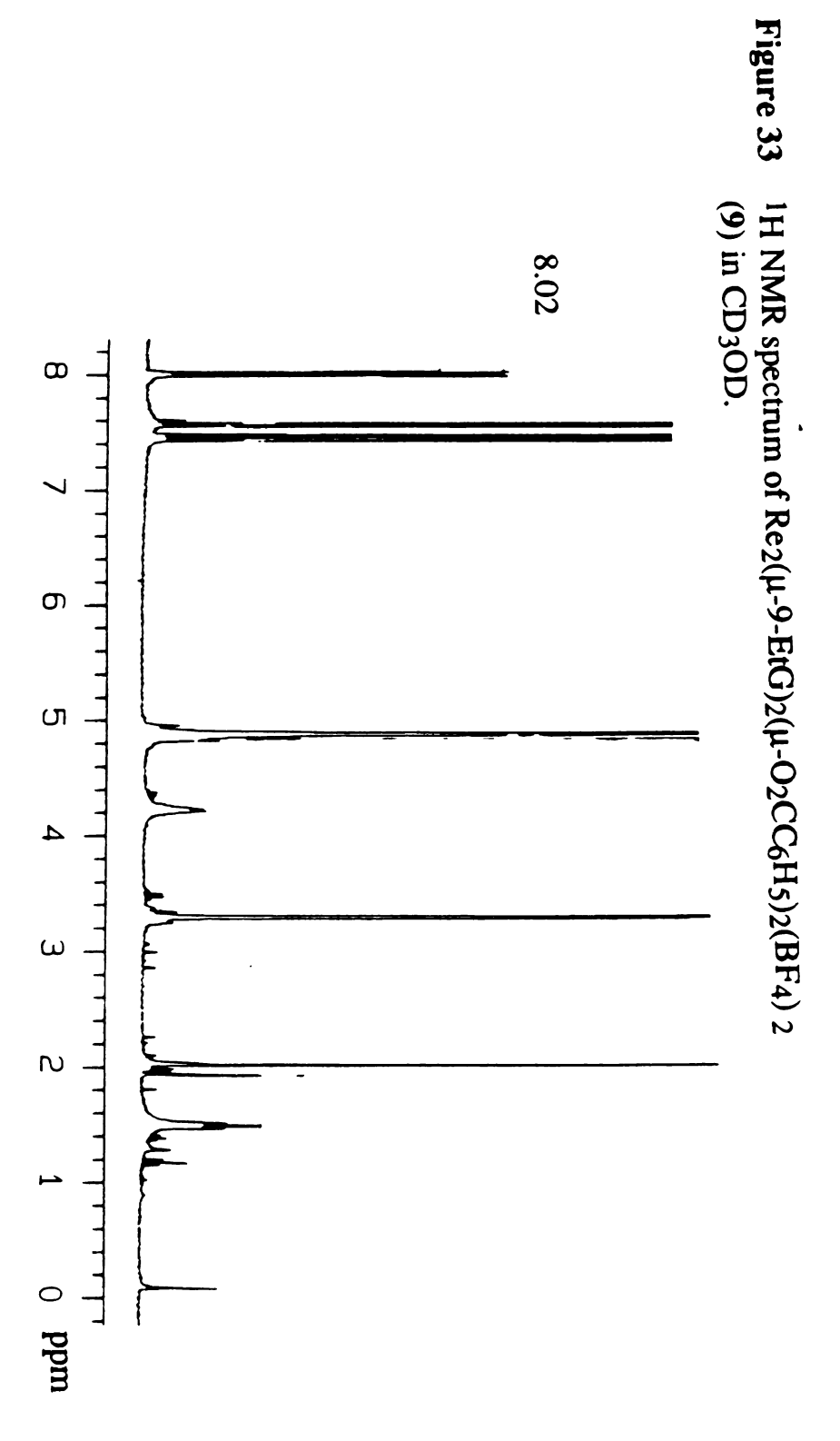
Figure 29

L = simultaneous substitution of the carboxylate ligands by 9-EtGH









#### List of References

- 1. (a) Rosenberg, B.; VanCamp, L. Nature 1969, 222, 385. (b) Thomson, A. Proceedings of the Second International Symposium on Platinum Coordination Complexes in Cancer Chemotherapy, Connors and Roberts, Ed.; Springer-Verlag; Berlin, 1974. (c) Eastman, A. Pharmac. Ther. 1987, 34, 155. (d) Pasini, A.; Zunino, F. Angew. Chem. Int. Ed. Engl. 1987, 26, 615 and references therein. (e) Frey, U.; Ranford, J. D.; Sadler, P. J. Inorg. Chem. 1993, 32, 1333 and references herein. (f) Howell, S. B., Ed. Platinum and Other Metal Complexes in Cancer Chemotherapy Plenum Press, New York, 1991. (g) Baker, S. A.-B.; Perez-Soler, R.; Khokhar, A. R. J. Coord. Chem. 1993, 29, 1. (g) McAuliffe, C. A.; Sharma, H. L.; Tinker, N. D. Chemistry of the Platinum Group Metals Recent Developments, Studies in Inorganic Chemistry 11, Hartley, F. R., Ed.; Oxford, New York, 1991, Ch.16. (h) Keppler, B. K. New J. Chem. 1990, 14, 389.
- 2. (a) Umapathy, P. Coord. Chem. Rev. 1989, 95, 129. (b) Lippard, S. J., Ed. Prog. Inorg. Chem. Wiley, New York, 1987, 37, 1 and references therein. (c) Sundquist, W. I.; Lippard, S. J. J. Coord. Chem. Rev. 1990, 100, 293 and references therein.
- 3. Lippard, S. J.; Berg, J. M. Principles of Bioinorganic Chemistry, Univ. Sci. Books; Mill Valley, CA; 1994.
- 4. (a) Burgess, J. Trans. Met. Chem. 1993, 18, 439. (b) Hollis, L. S.; Amundsen, A. R.; Stern, E. W. J. Med. Chem. 1989, 32, 136. (c) Allesio, E.; Balducci, G.; Calligaris, M.; Costa, G.; Attia, W. M.; Mestroni, G. Inorg. Chem. 1991, 30, 609.
- 5. (a) Harder, H. C.; Rosenberg, B. Int. J. Cancer. 1970, 6, 207. (b) Howle, J. A.; Gale, G. R. Biochem. Pharmocol. 1970, 19, 2757. (c)

- Sherman, S. E. Lippard, S. J. Chem. Rev. 1987, 87, 1153.
- 6. Reedijk, J. Pure & Appl. Chem. 1987, 59, 181.
- 7. Lippard, S. J. Pure & Appl. Chem. 1987, 59, 731.
- 8. Prescott, L. M.; Harley, J. P.; Klein, D. A. *Microbiology*, Wm. C. Brown Pub. New York, 1990, Ch. 10.
- 10. Howe-Grant, M. E., Lippard, S. J. Metal Ions in Biological Systems; Sigel, H., Ed.; Marcel Dekker; New York, 1980; Vol. 2, p.63.
- 12. (a) Pascoe, J.; Roberts, J Biochem. Pharmacol. 1974, 23, 1345. (b) Zwelling, L. Cancer Research 1978, 38, 1762 and references therein.
- 13. (a) den Hartog, J.; Altona, C.; van Boom, J.; van dere Marcel, A.; Reedijk, J. J. Am. Chem. Soc. 1984, 106, 1528. (b) den Hartog, J.; Altona, C.; Chottard, J.; Girault, J.; Lallemand, J.; DeLeeuw, F.; Marcelis, A.; Reedijk, J. Nucl. Acids Res. 1982, 10, 4715.
- 14. (a) Sherman, S. E.; Gibson, D.; Wang, A. H. -J.; Lippard, S. J. J. Am. Chem. Soc. 1988, 110, 7368. (b) Sherman, S.; Gibson, D.; Wang, A.; Lippard, S. Science, 1985, 230, 412 and references therein.
- 15. (a) van der Veer, J.; Ligtvoet, G.; van der Elst, H.; Reedijk, J. J. Am Chem. Soc. 1986, 108, 3860. (b) van der Veer, J.; van der Elst, H.; den Hartog, J.; Reedijk, J. Inorg. Chem. 1986, 25, 4657.
- 16. (a) Beck, D.; Brubaker, R. J. Bacteriol. 1973, 116, 1247. (b) Ciccarelli, R.; Solomon, M.; Varshavsky, A.; Lippard, S. Biochemistry 1985, 24, 7533. (c) Sundquist, W.; Lippard, S.; Stollar, B. Biochemistry 1986, 25, 1520.
- 17. (a) Dmitrov, N. V.; Eastwood, G. W. Current Chemother. Proc. Int. Cong. Chemother. 10th 1977. 1978, 2, 1319. (b) Eastland, G. W.; Yang, G.; Thompson, T. Meth. and Find. Exptl. Clin. Biochem. 1989, 10, 41.
- 18. (a) Erck, A.; Sherwood, E.; Bear, J. L.; Kimball, A. P. Cancer Res.

- 1976, 36, 2204. (b) Bear, J. L.; Gray, Jr., H. B.; Rainen, L., et. al. Cancer Chemotherapy Reports 1975, 59, 611. (c) Howard, R. A.; Spring, T. G.; Bear, J. L. Cancer Res. 1976, 36, 4402. (d) Chen, J.; Kostic, N. M. Inorg. Chem. 1988, 27, 2862.
- 19. Dunbar, K. R.; Matonic, J. H.; Saharan, V. P.; Crawford, C. A.; Christou, G. J. Am. Chem. Soc. 1994, 116, 2201.
- 20. (a) Köpf-Maier, P.; Köpf, H. Struct. Bond. 1988, 70, 104. (b) Köpf-Maier, P.; Köpf, H. Drugs of the Future 1986, 11, 297. (b) Kuo, L. Y.; Kanatzidis, M. G.; Sabat, M.; Tipton, A. L.; Marks, T. J. J.Am. Chem. Soc. 1991, 113, 9027 and references therein. (c) Heim, M. E.; Flechtner, H.; Keppler, B. K. Prog. Clin. Biochem. Med. 1989, 10, 217.
- 21. (a) Bear, J. L.; Howard, R. A.; Dennis, A. M. Curr. Chemother., Proc. Int. Cong. Chemother., 10th. 1978, 1977, 1321. (b) Rao, P. N.; Smith, M. L.; Pathak, S.; Howard, R. A.; Bear, J. L. J. Natl. Cancer Inst. 1980, 64, 905. (c) Bear, J. L.; Gray, H. B.; Rainen, L.; et al. Cancer Chemother. Rep. 1975, 59, 611. (d) Howard, R. A.; Spring, T. G.; Bear, J. L. Cancer Res. 1976, 36, 4402.
- 22. (a) Piraino, P.; Tresoldi, G.; Schiavo, S. L. Inorg. Chim. Acta 1993, 203, 101. (b) Schiavo, S. L.; Sinicropi, M. S.; Tresoldi, G.; Arena, C. G.; Piraino, P. J. Chem. Soc. Dalton Trans. 1994, 1517. (c) Fimiani, V.; Ainis, T.; Cavallaro, A.; Piraino, P. J. Chemother. 1990, 2, 319. (d) Piraino, P.; Bruno, G.; Tresoldi, G.; et al. Inorg. Chem. 1987, 26, 91.
- 23. TEXSAN-TEXRAY Structure Analysis package, Molecular Structure Corporation, 1985.
- 24. (a) MITHRIL: Integrated Direct Methods Computer Program, Gilmore, C. J. J. Appl. Cryst. 1984, 17, 42. (b) DIRDIF: Direct Methods for Difference Structures, An Automatic Procedure for Phase Extension;

- Refinement of Difference Structure Factors. Beurskens, P. T. Technical Report, 1984.
- 25. (a) Mann, B. E. Annual Reports on NMR Spectroscopy 1991, 23, 141
- and references therein. (b) Akermark, B.; Blomberg, M. R. A.; et al. J.
- Amer. Chem. Soc. 1986, 116, 3405. (c) Brown, T. H.; Green, P. J. J.
- Amer. Chem. Soc. 1970, 92, 2539. (d) Juranic', N. Coord. Chem. Rev.
- 1989, 96, 253. (e) Brevard, C.; Schimpf, R. J. Mag. Res. 1982, 47, 528.
- (f) Bonnaire, R.; Davoust, D.; Platzer, N. Org. Mag. Res. 1984, 22, 80.
- (g) Boyar, E. B.; Robinson, S. D. Inorg. Chim. Acta 1982, 64, L193. (h)
- Carr, C.; Glaser, J.; Sandstrom, M. Inorg. Chim. Acta 1987, 131, 153.
- 26. Cotton, F. A. and Walton, R. A. Multiple Bonds Between Metal Atoms Oxford Press, 2nd ed. 1993, and references therein.
- 27. (a) Webb, G. A. Annu. Rep. on NMR Spect. 1983, 14. (b) Garner, C.
- D.; Hughes, B. Adv. in Inorg. and Radiochem. 1975, 17, 1. (c) Matonic J.
- H.; Chen, S. J.; Pence, L. E.; Dunbar, K. R. Polyhedron 1992, 11, 541.
- 28. Dunbar, K. R.; Majors, S. O.; Sun, J. S. Inorg. Chim. Acta 1995, 229, 373.
- 29. Rempel, G. A.; Legzdins, P.; Smith, H.; Wilkinson, G. Inorg. Synth. 13, 90.
- 30. (a) Walton, R. A.; Srinivasan, V. Inorg. Chem. 1980, 19, 1635. (b)
- Cotton, F. A.; Oldham, C.; Walton, R. A. Inorg. Chem. 1967, 11, 214. (c)
- Cotton, F. A.; Oldham, C.; Walton, R. A. Inorg. Chem. 1966, 10, 1798.
- (d) Misailova, T. V.; Kotel'nikova, A. S. et al. Russ. J. Inorg. Chem. 1981, 26, 343 and references therein.
- 31. Cotton, F. A.; DeCanio, E. C.; Kibala, P. A.; Vidyasagar, K. *Inorg. Chim. Acta* 1991, 184, 221.

### **APPENDIX**

TABLES OF ATOMIC POSITIONAL PARAMETERS AND EQUIVALENT ISOTROPIC DISPLACEMENT PARAMETERS

**TABLE A.1.** Atomic positional parameters and equivalent isotropic displacement parameters ( $Å^2$ ) and their estimated standard deviations for  $[Rh_2(\mu-DTolF)_2(CH_3CN)_6][BF_4]_2$  (3).

atom	Х	у	Z	B(eq)
Rh(1)	0.63807(4)	0.14889(3)	0.10314(5)	1.71(3)
Rh(2)	0.56796(4)	0.14524(3)	-0.03820(5)	1.70(3)
N(1)	0.5862(4)	0.0990(3)	0.1470(5)	1.8(4)
N(2)	0.5077(4)	0.1109(3)	0.0413(5)	1.9(4)
N(3)	0.6278(4)	0.1766(3)	-0.1195(6)	3.0(5)
N(4)	0.5125(4)	0.1412(3)	-0.1654(6)	2.4(4)
N(5)	0.6158(4)	0.0904(3)	-0.0683(5)	2.0(4)
N(6)	0.5830(4)	0.1882(3)	0.1743(6)	2.4(4)
N(7)	0.6864(4)	0.1997(3)	0.0572(6)	2.3(4)
N(8)	0.7004(4)	0.1503(3)	0.2215(6)	2.3(4)
N(9)	0.6943(4)	0.1080(3)	0.0344(6)	1.9(4)
N(10)	0.5240(4)	0.2005(3)	-0.0081(6)	2.2(4)
<b>C</b> (1)	0.6088(5)	0.0694(3)	0.2157(7)	2.1(5)
C(2)	0.6234(5)	0.0276(4)	0.1911(8)	2.7(5)
C(3)	0.6138(5)	0.0821(3)	0.3075(7)	2.1(5)
C(4)	0.6452(5)	-0.0003(4)	0.258(1)	3.4(6)
C(5)	0.6345(6)	0.0530(4)	0.3722(7)	3.5(6)
<b>C</b> (6)	0.6492(5)	0.01606(4)	0.3487(9)	3.6(6)
<b>C</b> (7)	0.6721(7)	-0.0202(5)	0.420(1)	6.4(9)
C(8)	0.4467(5)	0.0997(4)	0.0147(6)	2.1(5)
C(9)	0.4101(5)	0.1300(3)	-0.0285(7)	2.6(5)
C(10)	0.3508(5)	0.1198(4)	-0.0602(7)	2.9(6)
<b>C</b> (11)	0.3253(5)	0.0789(4)	-0.0453(8)	3.1(6)
C(12)	0.2606(5)	0.0678(5)	-0.078(1)	4.7(7)
C(13)	0.3618(5)	0.0494(4)	0.0003(8)	2.9(5)
C(14)	0.4219(5)	0.0589(3)	0.0288(8)	2.8(5)
C(15)	0.5994(5)	0.0680(3)	-0.1498(7)	1.8(5)
<b>C</b> (16)	0.6327(5)	0.0738(4)	-0.2302(8)	3.9(6)
C(17)	0.6112(6)	0.0558(5)	-0.3111(8)	4.6(7)
C(18)	0.5571(5)	0.0316(4)	-0.3138(7)	3.0(6)
C(19)	0.5331(6)	0.0151(5)	-0.4040(9)	4.6(7)
C(20)	0.5268(5)	0.0258(3)	-0.2332(8)	2.6(5)
C(21)	0.5466(5)	0.0432(3)	-0.1515(7)	1.9(5)
C(22)	0.5310(5)	0.0907(3)	0.1139(7)	2.0(5)
C(23)	0.6557(6)	0.1925(5)	-0.178(1)	5.3(8)

TABLE A.1. continued.

atom	x	у	Z	B(eq)
C(24)	0.6902(8)	0.2139(8)	-0.251(1)	12(1)
C(25)	0.4863(6)	0.1358(3)	-0.2323(8)	3.1(6)
C(26)	0.4532(6)	0.1284(4)	-0.3223(8)	4.7(7)
C(27)	0.5590(6)	0.2118(4)	0.2213(8)	3.9(7)
C(28)	0.5275(7)	0.2416(6)	0.283(1)	8(1)
C(29)	0.7178(5)	0.2273(4)	0.0347(8)	2.9(6)
C(30)	0.7568(6)	0.2635(4)	0.007(1)	5.1(8)
C(31)	0.7585(5)	0.1026(3)	0.0605(6)	2.0(5)
C(32)	0.8019(5)	0.1293(4)	0.0233(8)	3.1(6)
C(33)	0.8629(6)	0.1269(4)	0.056(1)	3.9(6)
C(34)	0.8798(6)	0.0986(4)	0.1251(9)	3.6(6)
C(35)	0.9452(7)	0.0987(5)	0.163(1)	7(1)
C(36)	0.8355(6)	0.0712(4)	0.1574(8)	3.5(6)
C(37)	0.7748(5)	0.0728(3)	0.1271(7)	2.4(5)
C(38)	0.7372(6)	0.1476(4)	0.2762(7)	3.0(5)
C(39)	0.7862(7)	0.1446(5)	0.3475(8)	5.5(7)
C(40)	0.4940(6)	0.2299(4)	0.0008(7)	2.8(6)
C(41)	0.4568(6)	0.2690(4)	0.015(1)	5.3(8)
C(42)	0.6722(5)	0.0859(3)	-0.361(7)	2.2(5)
$\mathbf{B}(1)$	0.356(1)	0.2409(8)	0.746(2)	7.1(5)
B(2)	0.604(1)	0.1716(6)	0.516(1)	5.3(4)
F(1)	0.5908(5)	0.1937(3)	0.5897(7)	10.5(7)
F(2)	0.6595(4)	0.1501(3)	0.5290(8)	9.5(6)
F(3)	0.5588(5)	0.1439(4)	0.4974(8)	11.2(7)
F(4)	0.6111(6)	0.1982(4)	0.4455(8)	11.5(8)
F(5)	0.3365(6)	0.2131(4)	0.6836(8)	13(1)
F(6)	0.3072(6)	0.2631(4)	0.771(1)	15(1)
F(7)	0.3847(7)	0.2232(4)	0.810(1)	15(1)
F(8)	0.3923(6)	0.2715(4)	0.704(1)	13(1)
H(1)	0.6181	0.0181	0.1297	3.3
H(2)	0.6035	0.1104	0.3254	2.6
H(3)	0.6575	-0.0281	0.2396	4.1
H(4)	0.6383	0.0616	0.4343	4.3
H(5)	0.6454	-0.0444	0.4212	7.7
H(6)	0.7126	-0.0289	0.4052	7.7
H(7)	0.6717	-0.0067	0.4784	7.7
H(8)	0.4254	0.1580	-0.0380	3.2
H(9)	0.3271	0.1405	-0.0920	3.4
H(10)	0.2431	0.0919	-0.1084	5.7

TABLE A.1. continued.

atom	x	у	Z	B(eq)
H(11)	0.2630	0.0446	-0.1207	5.7
H(12)	0.2538	0.0599	-0.0278	5.7
H(13)	0.3455	0.0218	0.0120	3.5
H(14)	0.4456	0.0375	0.0582	3.3
H(15)	0.6699	0.0894	-0.2297	4.7
H(16)	0.6338	0.0598	-0.3666	5.5
H(17)	0.4970	-0.0009	-0.3936	5.6
H(18)	0.5246	0.0386	-0.4431	5.6
H(19)	0.5639	-0.0025	-0.4315	5.6
H(20)	0.4904	0.0089	-0.2335	3.2
H(21)	0.5240	0.0381	-0.0969	2.4
H(22)	0.5068	0.0694	0.1428	2.5
H(23)	0.7314	0.2018	-0.2525	14.2
H(24)	0.6704	0.2075	-0.3070	14.2
H(25)	0.6924	0.2430	-0.2401	14.2
H(26)	0.4130	0.1399	-0.3166	5.8
H(27)	0.4747	0.1424	-0.3705	5.8
H(28)	0.4514	0.0988	-0.3336	5.8
H(29)	0.5569	0.2546	0.3209	9.4
H(30)	0.5069	0.2626	0.2465	9.4
H(31)	0.4974	0.2270	0.3194	9.4
H(32)	0.7815	0.2718	0.0578	6.2
H(33)	0.7821	0.2542	-0.0418	6.2
H(34)	0.7316	0.2865	-0.0119	6.2
H(35)	0.7911	0.1490	-0.0237	3.7
H(36)	0.8938	0.1451	0.0301	4.6
H(37)	0.9479	0.774	0.2090	7.9
H(38)	0.9279	0.0927	0.1147	7.9
H(39)	0.9534	0.1259	0.1883	7.9
H(40)	0.8469	0.0504	0.2021	4.3
H(41)	0.7446	0.0539	0.1515	2.9
H(42)	0.7670	0.1433	0.4058	6.7
H(43)	0.8094	0.1197	0.3367	6.7
H(44)	0.8123	0.1691	0.3446	6.7
H(45)	0.4829	0.2922	0.0292	6.3
H(46)	0.4358	0.2746	-0.0416	6.3
H(47)	0.4283	0.2639	0.0619	6.3
H(48)	0.6987	0.0659	-0.0649	2.6
H(49)	0.6638	0.2172	-0.1386	5.8



TABLE A.1. continued.

atom	X	y	Z	B(eq)	
H(50)	0.6895	0.1730	-0.1681	5.8	
H(51)	0.4907	0.1654	-0.2486	3.1	
H(52)	0.5222	0.1211	-0.2585	3.1	
H(53)	0.5191	0.2049	0.1928	4.4	
H(54)	0.5627	0.1917	0.2724	4.4	
H(55)	0.6819	0.2442	0.0184	3.0	
H(56)	0.7270	0.2338	0.0981	3.0	
H(57)	0.7685	0.1573	0.2330	3.3	
H(58)	0.7219	0.1731	0.3064	3.3	
H(59)	0.5065	0.2323	0.0648	2.8	
H(60)	0.5232	0.2470	-0.0339	2.8	



